A senescence-mimicking (senomimetic) VEGFR TKI side-effect primes tumor immune responses via IFN/STING signaling

Melissa Dolan, Yuhao Shi, Michalis Mastri, Mark Long, Amber Mckenery, James Hill, Cristina Vaghi, Sébastien Benzekry, Joseph Barbi, John Ebos

A senescence-mimicking (senomimetic) VEGFR TKI side-effect primes tumor immune responses via IFN/STING signaling.

Melissa Dolan[1], Yuhao Shi[1], Michalis Mastri[2], Mark Long[3], Amber McKenery[2], James W. Hill[4], Cristina Vaghi[5,6], Sebastien Benzekry[5,6], Joseph Barbi[7], and John M.L. Ebos[1,2,8, 9*]

1 Department of Experimental Therapeutics, Roswell Park Comprehensive Cancer Center Buffalo, NY, 14263. USA
2 Department of Cancer Genetics and Genomics, Roswell Park Comprehensive Cancer Center, Buffalo, NY, 14263. USA
3 Department of Bioinformatics and Statistics, Roswell Park Comprehensive Cancer Center Buffalo, NY, 14263. USA
4 Jacobs School of Medicine and Biomedical Sciences, SUNY at Buffalo Buffalo, New York, 14263. USA
5 Inria Team MONC, Inria Bordeaux Sud-Ouest, Talence, France
6 Computational Pharmacology and Clinical Oncology (COMPO), Inria Sophia Antipolis–Méditerranée, Cancer Research Center of Marseille, Inserm UMR1068, CNRS UMR7258, Aix Marseille University UM105, 13385 Marseille, France
7 Department of Immunology, Roswell Park Comprehensive Cancer Center Buffalo, NY, 14263. USA
8 Department of Medicine, Roswell Park Comprehensive Cancer Center Buffalo, NY, 14263. USA
9 Lead Contact

* Correspondence: John M.L. Ebos, Roswell Park Comprehensive Cancer Center, Center for Genetics and Pharmacology, Elm and Carlton Streets, Buffalo, NY 14263. Phone: 716-845-8233; E-mail: John.Ebos@RoswellPark.org

Running Title: Senescence-mimicking treatments drive tumor immune responses

Conflict of Interest: None

Abstract

Tyrosine kinase inhibitors (TKIs) that block the vascular endothelial growth factor receptors (VEGFRs) disrupt tumor angiogenesis but also have many unexpected side-effects that impact tumor cells directly. This includes the induction of molecular markers associated with senescence, a form of cellular aging that typically involves growth arrest. We have shown that VEGFR TKIs can hijack these aging programs by transiently inducting senescence-markers (SMs) in tumor cells to activate senescence-associated secretory programs that fuel drug resistance. Here we show that these same senescence-mimicking ('senomimetic') VEGFR TKI effects drive an enhanced immunogenic signaling that, in turn, can alter tumor response to immunotherapy. Using a live-cell sorting method to detect beta-galactosidase, a commonly used SM, we found that subpopulations of SM-expressing (SM+) tumor cells have heightened interferon (IFN) signaling and increased expression of IFN-stimulated genes (ISGs). These ISG increases were under the control of the STimulator of INterferon Gene (STING) signaling pathway, which we found could be directly activated by several VEGFR TKIs. TKI-induced SM+ cells could stimulate or suppress CD8 T-cell activation depending on host:tumor cell contact while tumors grown from SM+ cells were more sensitive to PD-L1 inhibition *in vivo*, suggesting that offsetting immune-suppressive functions of SM+ cells can improve TKI efficacy overall. Our findings may explain why some (but not all) VEGFR TKIs improve outcomes when combined with immunotherapy and suggest that exploiting senomimetic drug side-effects may help identify TKIs that uniquely 'prime' tumors for enhanced sensitivity to PD-L1 targeted agents.

Significance Statement:

This study identifies an unexpected tumor-intrinsic side-effect of TKIs typically associated with targeting angiogenesis that can modulate nearby immune cell activity by increasing senescence-marker expression and promoting IFN/STING signaling.

Introduction

There is an ongoing and rapidly expanding search for drugs that can improve outcomes in cancer patients when combined with immune checkpoint inhibitors (ICIs) that block the programmed cell-death 1 (PD-1) pathway[1]. Tyrosine kinase inhibitors (TKIs) that target vascular endothelial growth factor receptors (VEGFRs) to limit tumor angiogenesis are now the drug class tested in the highest frequency with ICIs in active clinical trials worldwide[1]. Yet a molecular basis to explain why VEGFR TKI and ICI combinations work remains unclear, particularly why only some VEGFR TKIs seem to yield improved responses/reduced toxicity over others, despite often having similar target profiles[2,3]. One explanation may include senescence, a cellular stress response that limits proliferation by forcing growth arrest in the G1 or G2/M stage. The induction of senescence is a common side-effect for many cancer drugs, and several senescence-markers (SMs) are used as surrogates to identify cells undergoing this process[4]. SMs include increases in cyclin-dependent kinases, senescence-associated (SA) β-galactosidase (SA-β-gal), and SA secretory phenotypes (SASPs), amongst several others[4,5]. But the use of SMs to define senescence remain imperfect as numerous cancer drugs can force SM expression and co-opt features of senescent cells but, ultimately, elude permanent growth arrest[6]. We recently reported that VEGFR TKIs have this senescence-mimicking ('senomimetic') drug property as they are well known to induce SMs, but we found these cellular features eventually diminish when treatment is removed[7,8].

To date, attempts to assess the full impact of senomimetic drug effects remain uncertain as actual therapy-induced senescence (i.e, including permanent growth arrest) can have enigmatic, if not contradictory, effects on tumor growth[9-11]. Cellular stasis (even temporary) and SASPs can limit *and* promote tumor growth simultaneously, therefore senescence has been linked to both drug efficacy and resistance[12-15]. More recently, these paradoxical opposing effects of senescence on cancer progression can also include immune responses[12,16]. Senescent cells can *promote* innate and adaptive immunity via natural killer cells[17-20], macrophages[21,22], neutrophils[23], and CD4/CD8 T-cells[18,23,24]; while senescent cells can also *suppress* immunity by increasing NK-blocking non-classical MHC molecules[24] or the production of myeloid cell-attracting proteins such as IL-6[25]. This raises the question of whether the senomimetic effects of VEGFR TKIs might also be able to modulate the cellular signaling that regulate both immune/senescence pathways in tumor cells, possibility impacting immunotherapy efficacy. In

this regard, interferon (IFN) signaling might be a candidate as it can regulate both immunity and senescence. For instance, IFN signaling and the STING (STimulator of INterferon Gene) pathway can control immune activation in senescent cells via SASPs, antigen presentation, and immune-checkpoint ligand expression (i.e., PD-L1)[12,16,26-36].

To evaluate this further, we examined the link between the transient senomimetic consequences of VEGFR TKI treatment and the immune-modulating factors controlled by IFN/STING signaling in an effort to explain why combinations with ICIs yield improved benefits[37-40]. To do this we first used a live-cell sorting method to identify SM-expressing (SM+) cells based on SA-β-gal expression, and then compared immune phenotype of SM+ cells after VEGFR TKI treatment. Our results identified a novel IFN-enriched gene signature specific to SM+ cells that we validated using published clinical and preclinical datasets involving treatment with various TKIs. Numerous VEGFR TKIs were found to induce IFN stimulated genes (ISGs) *and* SM-expression, which we linked to the direct activation of STING signaling. Critically, ISGs expressed by SM+ cells had contrasting immune-stimulatory and -inhibitory effects, which we discovered could be offset by PD-L1 inhibition *in vivo*. Together, these results suggest that the induction of STING-controlled SM-expressing cell populations by VEGFR TKIs 'prime' tumors for combinatorial efficacy with PD-1 pathway inhibitor treatments in patients.

Results

IFN signaling is enriched in senescence marker (SM) expressing tumor cells after TKI treatment.

We previously reported that VEGFR TKI treatments transiently induce expression of several hallmark SMs, including upregulated p21, cell size increase, G1 arrest, and a tumor-promoting secretory program closely resembling SASPs[7]. VEGFR TKIs also strongly induce SA-β-gal, a hydrolase enzyme located in lysosomes and commonly used as a SM[7,41]. Here we used a fluorescent substrate for SA-β-gal (C_{12}FDG)[42,43] to isolate live SM-expressing cell populations to assess changes in immune-related genes after short- and long-term VEGFR TKI treatment periods. Short-term treatments included drug administration to tumor cells for 48hrs *in vitro* while long-term treatments utilized TKI-resistant (R) cells derived *in vivo*[7] (**Fig 1A: schematic shown in S1A)**. Using a previously established methodology[7], an example of live-cell sorting using axitinib (Ax) resistant (AxR) mouse breast 4T1 model is shown in **Fig 1B (See Appendix 1 for gating strategy)** where FACS-isolated SA-β-gal expressing cell populations were separated based on high and low SM expression (SM+ and SM-, respectively). As evidence that the senomimetic drug effects are transient and lack growth arrest, $4T1^{AxR}$ SM+ cells continued proliferating and remained viable similar to $4T1^{AxR}$ SM- after FACS-isolation (**Fig 1C**). To investigate a potential link between SM expression and immune-related genes, we performed whole genome RNA-seq analysis on isolated $4T1^{AxR}$ SM+/SM- cell populations (**Fig 1D**). $4T1^{AxR}$ SM+ cells had several unique differentially-expressed genes (DEGs) compared to non-resistant parental 4T1 ($4T1^{P}$) and $4T1^{AxR}$ SM- cells (**Fig 1E**). Gene ontology (GO) analysis showed $4T1^{AxR}$ SM+ cells to be enriched for biological processes associated with senescence and immunity (both adaptive and innate; **Fig 1F**). Similarly, gene set enrichment analysis (GSEA) showed SM+ cells to have significant enrichment for senescence-associated genes and immunity-associated genes[11,44-51] (**Fig. 1G; genesets explained in Table S1**). Interestingly, GSEA also revealed positive enrichment for type I and II IFN pathways in $4T1^{AxR}$ and $4T1^{AxR}$ SM+ cells (**Fig 1H**), a result we confirmed using the interferome database[52] which showed upregulation of several IFN-regulated genes (**Fig 1I; see Methods for database details**). Upregulation of numerous interferon-stimulated genes (ISGs) such as *Ifit1*, *Ifit2*, *Ifit3*, *Irf7*, and *Rsad2* were further confirmed in $4T1^{AxR}$ (**Fig 1J;** compared to P) and $4T1^{AxR}$ SM+ cells (**Fig 1K;** compared to SM-). Short-term Ax treatment *in vitro* produced similar IFN signaling

enhancement in 4T1 (**Fig 1L)** and 4T1 SM+ cell populations **(Fig 1M)**. We separately verified these results using multiple drugs, cell lines, and treatment conditions (**described in Supplemental Result section and Figs S1B-M**). For example, VEGFR TKIs such as cabozantinib (Ca), Tivozanib (Tivo), Pazopanib (Pazo), and Lenvatinib (Len) all significantly increased SM expression in 4T1 cells, with Ax, Ca, and Len among the most robust (**Fig 1N; Fig S1B shows optimal dose determination**). Also, because Ca has unique drug-targets beyond VEGFRs (i.e, c-MET, AXL, etc.[53]), Ca-resistant (CaR) and short-term Ca treatment models were found to also yield ISG- and SM-expression increases in EMT6 cells, an additional mouse breast cancer model (**Fig S1C, for derivation of EMT6^{CaR} variants; Figs S1D-E, for ISG-/SM-expression).** Further confirmations of TKI-induced SM and ISG expression were performed in a human breast tumor cell line (LM2-4) and a non-breast mouse kidney tumor cell line (RENCA) (**Fig S1H-L; described in Supplemental Results**). Together, these results demonstrate that a broad drug-class side-effect of TKIs typically associated with VEGFR blockade can include direct-tumor cell effects that induce ISG- and SM-expression.

Identification and validation of an IFN-enriched SM gene score induced by VEGFR TKIs

We next examined whether IFN-enrichment found in SM+ cells can be validated/confirmed in publicly available clinical and preclinical transcriptomic datasets from VEGFR TKI-treated samples. First, we examined two clinical datasets that included tumor biopsies taken before and after neoadjuvant TKI treatment. These included 20 Pazo-treated renal cell carcinoma (RCC) patients (Wood *et al*.[54]) and 7 sunitinib (Su)-treated breast cancer (BC) patients (Braga *et al*.[55]). GSEA revealed IFN responses are enriched after Pazo and Su treatment **(Fig 2A and 2B; see methods for details)**. Next, two preclinical datasets were similarly compared and IFN responses were also found to be enriched in Su-treated RCC patient derived xenografts (PDXs) (**Fig 2C**, Diaz-Montero *et al*.[56]) and in Su-Resistant (SuR) LM2-4 cells (**Fig 2D**, Mastri *et al*.[7]). To confirm IFN gene enrichment was specific to TKI-induced SM+ cell populations, we generated an IFN-enriched gene score specific to SM+ cell populations. This was done by identifying unique gene signatures exclusive to SM+ (**Fig S2A**) and SM- cells (**Fig S2B**), and then using a T-score analysis to obtain a 'SM+ T-score' that could be examined in TKI-treated patient data (**Fig 2E; see methods for analysis details and Table S2 for signature details**). The SM+ T-score was found to increase in 4/5 matched pre-/post-treatment RCC samples (**Fig 2F**) and be

enriched in 13/17 post-treatment RCC samples (**Fig 2G**). Similarly, the SM+ T-score increased in 2/4 matched pre-/post-treatment BC samples (**Fig 2H**) and was enriched in 5/7 post-treatment BC samples (**Fig 2I**). Together, these results confirm the link between TKI-induced SM-expression and immunity, and demonstrate genes specific to SM+ and IFN-expression are enriched by multiple TKIs, clinically and preclinically, in multiple cancer types.

TKI-induced SM expression can be regulated by a STING-IFNβ signaling axis

Since STING can be a potent regulator of type I IFNs, ISGs, and senescence[27,28,33,57], we examined STING expression following VEGFR TKI treatment. In a model representing long-term drug exposure, $4T1^{AxR}$ cells were found to have increases in phosphorylated STING (pSTING) and in TBK1 (pTBK1), which is activated by STING (**Fig 3A and 3B; Fig S3A shows densitometry analysis and statistics summary; Appendix 2 shows blotting replicates**). Next, to directly link STING pathway activation with senomimetic effects, we treated 4T1 cells with STING agonists such as MSA-2[57] and DMXAA[58,59] and found SM-expression increases (**Fig 3C**). Interestingly, STING activity or expression was directly increased after treatment with multiple TKIs in 4T1 cells, with Ax and Ca showing levels similar to (or greater than) DMXAA/MSA-2 compared to vehicle controls (**Fig 3D; Fig 3E for densitometry analysis; Fig S3B for statistics summary**). We next tested whether STING could control Ax-induced ISGs and SM-expression by knocking down STING expression in 4T1 cells via short hairpin RNA (referred to as STING-KD; **see Methods for details).** Critically, $4T1^{STING\text{-}KD}$ cells had decreased TKI-induced STING expression and activation (**Fig 3F**), decreased ISG levels (**Fig 3G**), and decreased SM-expression (**Fig 3H**) compared to vector controls. These results were confirmed in $EMT6^{CaR}$ cells where increases in SM-expression (**Fig 3I**) and activated pSTING and pTBK1 (**Figs 3J and 3K**) could be reversed after treatment with a STING antagonist SN-011 **(Figs 3I-K; Fig S3C shows densitometry analysis and statistics summary; Appendix 2 shows blotting replicates).** Notably, in EMT6 cells the STING pathway activation induced by long-term TKI treatment **(Fig. 3J)** was not consistently observed by short-term treatment, indicating that longer drug exposure times are required to observe this effect in some cell lines (**Fig S3D; Fig S3E for statistics summary**). Together, these results demonstrate that STING can contribute to TKI-induced SM-expression and ISG levels in 4T1 and EMT6 tumor cells. Next, since STING activation can drive production/activation of IFNs[27,60,61], we evaluated IFN signaling and IFN

treatment response as a surrogate for STING modulation by TKI treatment. Similar to other studies[27,28,33], we found IFN stimulation (both type I and II) could increase SM-expression in 4T1 cells (**Fig 3L**). Interestingly, we found only IFNβ levels were increased in 4T1 cells after short-term Ax-treatment (**Fig 3M**), a result we confirmed in $4T1^{AxR}$ and $EMT6^{CaR}$ cells (**Figs S3F and S3G, respectively**). These results suggest that STING-modulation by TKI treatment may have specific consequences unique to IFNβ. To confirm this, we examined Ax-treated $4T1^{STING\text{-}KD}$ cells and found IFNβ level increases were partially reversed (**Fig 3N**). Together, these results suggest that Ax-induced SM-expression might be regulated by a STING-IFNβ signaling response via an autocrine mechanism. To test this, we examined type I IFN signaling regulation of SM-expression in EMT6 cells because short-term treatment did not induce STING pathway activation. Using EMT6 cells with the receptor for type I IFNs (IFNAR1) knocked down ($EMT6^{IFNAR1\text{-}KD}$), we found Ax- and Ca-induced SM-expression was reduced compared to vehicle-treated (**Fig 3O)** and vector controls (**Fig S3H)**, thus confirming IFN-signaling machinery is a modulator of TKI-induced SM-expression. Together these results identify a novel side-effect of VEGFR TKI treatment involving the activation of a STING-IFNβ signaling axis that can drive SM-expression in tumor cells. The magnitude of this effect was confirmed in multiple systems and found to vary based on TKI-type, treatment duration, and tumor model.

SM+ cells can express immune regulators with opposing functions.

Since ISGs involved in senescence and immunity can sometimes have opposing/contradictory functions that both promote and inhibit tumor growth[28,61-63], we examined various antigen presentation genes and immune-regulating surface proteins after TKI-treatment. First, we found Tap1 (transporter protein supporting antigen processing) and H2d1/B2m (MHC class I molecules) significantly increased in Ax-treated 4T1 cells (**Fig 4A)**. Notably, this effect could be partially reversed in Ax-treated $4T1^{STING\text{-}KD}$ cells (**Fig 4B**). Ca-treatment also significantly increased at least one antigen presentation marker in 4T1 or EMT6 cells **(Figs S4A and S4B, respectively**) and in human LM2-4 cells where HLA-A/B/C were also tested and found to increase (**Fig S4C**). Similar antigen presentation gene increases were found in $4T1^{AxR}$ cells (compared to $4T1^{P}$) and in $4T1^{AxR}$ SM+ cells (compared to SM- cells), suggesting there can be a magnification of this effect in SM-expressing cells after long-term TKI treatment **(Fig 4C and 4D, respectively; $EMT6^{CaR}$ shown in Fig S4D).** Based on these results, we further examined

surface expression of ISGs at the protein level in SM-expressing cells known for immune-regulatory functions and links to senescence and immunotherapy[64]. This included MHC-I (an immune-promoter) and PD-L1 (an immune-suppressor) which were evaluated by flow cytometry after TKI treatment. Both Ax or Ca treatment significantly increased MHC-I in 4T1 (**Fig 4E; representative histogram example shown**) and PD-L1 (**Fig 4F; representative histogram example shown**) compared to untreated controls. Like MHC-I class genes, Ax-induced PD-L1 expression increases could be partially reversed in $4T1^{STING\text{-}KD}$ cells (**Fig S4E**). Importantly, using C_{12}FDG to gate for SA-β-gal expression in 4T1, surface MHC-I and PD-L1 levels could be compared in SM+/SM- cell populations (**Fig 4G, gating schematic and representative histograms shown**). Using this method, SM+ gated cell populations were found to have significantly increased MHC-I **(Fig 4H)** and PD-L1 **(Fig 4I)** compared to SM- gated cells after Ax and Ca treatment in 4T1 cells. Studies conducted in TKI-resistant cells showed similar MHC-I and PD-L1 level increases in SM+ gated cells from $4T1^{AxR}$ (**Fig S4F; representative histogram shown**) and $EMT6^{CaR}$ (**Fig S4G**) tumor cells compared to SM- gated cells. Together, these results demonstrate that TKI-induced senomimetic effects can modulate expression of cell-surface ISGs that can be key immune-regulators with dual (and opposing) functions on tumor-controlling in PD-1+ T-cell activity.

SM+ tumor cell immunogenicity overcomes secretome-mediated suppression of CD8 T-cells

To assess whether these TKI-induced SM+ cells have altered immune-modulating potential, we examined tumor growth in models of varied adaptive immune response capabilities. We know based on our prior studies that when FACS-isolated $4T1^{AxR}$ SM+ tumor cells are orthotopically implanted into immune-*competent* Balb/c mice, SM+ tumors can have a growth advantage over SM- tumors because of a tumor-promoting secretory profile (**Fig. 5A-left**; similar data published in[7]). To test whether the presence of immune cells can impact this growth, $4T1^{AxR}$ SM+/SM- cells were implanted into 1) immune-*compromised* SCID mice, which lack mature B- and T-cells **(Fig. 5A-middle**); or 2) Balb/C mice treated with a T-cell inhibiting αCD8 antibody (**Fig 5A-right; CD8 T-cell depletion confirmed in Appendix 3**). In both immune-depleted models, SM+ tumor growth advantages significantly increased compared to SM- controls as shown by mixed-effects analysis using a reduced Gompertzian model to compare tumor growth rates,

which is measured by a 'β' parameter value[65] (**Fig 5B; red bars represent fold-change in β compared to SM- tumors; β analysis explained in Appendix 4**). These data show that SM+ tumor growth is more sensitive to immune cell control and raise the question of whether known tumor-promoting secretome programs may be offset by surface-expressing proteins that control immune response. To examine this further, we evaluated CD8 T-cell activation *ex vivo* using conditioned media (CM) or co-cultures to assess contact-independent (secretory) and contact-dependent effects of TKI-resistant tumor cells on CD3/CD28 stimulated splenocytes from Balb/c mice. Measurements included CD8+ T-cell proliferation[66], and T-cell effector proteins such as Granzyme B (GRMB) and IFNγ that are capable of tumor cell-killing[67] (**Fig 5C; schematic shown; see Appendix 5 for gating strategy**). In studies comparing $4T1^{AxR}$ or $EMT6^{CaR}$ variants to controls, CM increased CD8 T-cell proliferation and at least one marker of tumor cell-killing (**Fig 5D for AxR; Fig S5A for CaR; Fig S5C and S5E show non-normalized data**). Similarly, when the same TKI-resistant cells were co-cultured, activated CD8 T-cell levels were also increased, suggesting a generalized T-cell activating (and immune-promoting) effect of VEGFR TKI treatment on tumor cells regardless of cell-contact (**Fig 5E**; **Fig S5B for CaR; Fig S5D and S5F show non-normalized data)**. Yet when we performed similar studies using FACS isolated SM+/SM- cell populations, we found an opposite effect (**Fig 5F; schematic shown**). In this case, we found the CM of $4T1^{AxR}$ SM+ and $EMT6^{CaR}$ SM+ cells were immune-suppressing, and able to significantly decrease CD8 T-cell proliferation and cell-killing protein expression (**Fig 5G; Fig S5G for $EMT6^{CaR}$ SM+; Fig S5I and S5K show non-normalized data)**. Critically, this suppressive effect of SM+ cells was reversed or diminished when co-cultured with splenocytes (**Fig 5H; Fig S5H for $EMT6^{CaR}$ SM+; Fig S5J and S5L show non-normalized data**). Together, these results show that long-term TKI-treatment can induce an overall immune promoting effect in tumor cells, with co-culture or CM showing at least one increased marker for T-cell activation (**Fig 5I shows summary heatmaps**). Yet, when these same cells are separated based on SM-expression, a complex context-dependent role emerges, with SM+ tumor cell populations having a secretory-based immune suppressive effect that can be counteracted when the same SM+ cells are in direct contact with activated splenocytes (**Fig 5J; graphical summary shown in 5K**). Together, these results demonstrate that the senomimetic properties of TKIs can have dual consequences on CD8 T-cell activation and immune-regulated tumor growth, with

tumor-promoting secretory properties of SM+ cell populations overshadowed by immune-promoting contact-dependent protein expression.

SM+ tumors have increased sensitivity to PD-L1 inhibition

Because TKI-induced SM-expressing cells simultaneously express MHC-I and PD-L1, ISGs with opposing roles in T-cell activation, we tested whether PD-L1 pathway inhibition could limit the immune-suppressing senomimetic effects of TKIs and boost overall anti-tumor outcomes *in vivo*. To do this, we first confirmed tumors grown *in vivo* have increased SM-expressing subpopulations of cells after VEGFR TKI treatment (**Fig 6A; Ax treatment and 4T1 model used**). Next, we treated Balb/c mice bearing orthotopically-grown 4T1 tumors with Ax or a PD-L1 neutralizing antibody (αPD-L1) alone or in combination (**Fig 6B**) and found αPD-L1 treatment induced significant tumor inhibition when combined with Ax after 29 days (**Fig 6C**). Notably, cumulative anti-tumor growth rates were significantly different compared to vehicle controls at various timepoints (**Fig S6A for statistics summary**) but were minimal overall across all treatments (**Fig 6D**) – a finding consistent with reported lack of responses to immune-checkpoint inhibitors in the 4T1 model[68]. Because of this, and reported instances of fatal hypersensitivity to long-term exposure to antibodies targeting the PD-1 pathway in 4T1 models[69,70], we utilized the EMT6^{CaR} tumor model to more directly assess the impact of PD-L1 inhibition on SM-expressing subpopulations as EMT6^{CaR} SM+ cells also had a significant growth advantage *in vitro* and *in vivo* compared to SM- cells (**Fig S6B-D**). When EMT6^{CaR} SM+ and SM- tumor cells were orthotopically implanted into Balb/c mice, we found only SM+ tumors were significantly inhibited by αPD-L1 treatment (**Fig 6E**), with the magnitude of tumor inhibition significantly increased compared to EMT6^{CaR} SM- tumors (**Fig 6F; SM+ treated vs. SM- treated comparison**). Together, these results indicate that SM+ tumors can be more sensitive to anti-PDL1 antibody treatment and suggest that the senomimetic effects of TKIs may be responsible, at least in part, for tumor response to immune checkpoint inhibition via αPD-L1 antibody treatment (**Fig G shows schematic summary**).

Discussion

VEGFR TKIs and immune-checkpoint inhibitors are approved in combination to treat multiple metastatic cancers[71-74]. While VEGFR TKIs are typically associated with blocking tumor angiogenesis, all TKIs have a myriad of off-target side-effects that alter processes directly in the tumor itself. This study investigated a VEGFR TKI side-effect involving senescence, a part of the aging process that can have enigmatic, if not contradictory, effects on tumor growth and immunity. VEGFR TKIs can temporarily hijack the senescence-machinery[7,8] and may drive immune/tumor-modulating processes[75,76], but the consequences of SM induction remain understudied in the context of ICI efficacy. Using multiple drugs and tumor models, we performed transcriptomic and proteomic analysis to show that VEGFR TKI-induced SM+ tumor cells increase expression of multiple cell-surface ISGs known to regulate immunogenicity, many of which we found to be controlled by type I IFN and STING signaling. Notably, SM+ cells could functionally alter CD8 T-cell activity in a context-dependent manner and SM+ tumors were more sensitive to PD-L1 inhibition *in vivo,* suggesting that the senomimetic side-effects of VEGFR TKIs include direct tumor-intrinsic activation of IFNs/STING programs that could be exploited to optimally select TKIs to pair with ICIs to improve patient outcomes.

There is growing interest in therapy-induced senescence (TIS) and the implications for cancer progression[77], with efforts to develop drugs that can suppress the negative effects of senescent cells (senomorphics) or kill them completely (senolytics)[78,79]. But strict definitions of senescence remain elusive[80]. Surrogate markers of senescence can be expressed differentially based on drug type and dose, duration of treatment, cell and model system, amongst many other hallmarks that are independent of permanent growth arrest[4]. Indeed, dedicated efforts such as the Cellular Senescence Network (SenNet) are currently seeking to standardize definitions of senescence, but the question of whether cellular stasis or senescence phenotypes are permanent remain controversial[81,82]. For instance, several cancer therapies drive tumor cells into a state resembling or mimicking cellular senescence, often described as ‘senescence-like’ or ‘pseudo-senescence’, or generally as an ‘incomplete’ process [7,83,84]. Similar to what we describe here with VEGFR-targeted drugs, these senomimetic molecular changes can be exhibited by TKIs such as those that target CDK4/6[85,86], PARP[87], BRAF[88] and EGFR[83,89] suggesting this could be a conserved cellular response to cancer therapy, where treated tumor cells can be re-wired to mimic senescent cells to survive treatment-induced stress. As an example, palbociclib (a

CDK4/6 inhibitor) can cause hepatocellular cancer cells to mimic senescent cells *in vitro* and *in vivo*, ultimately contributing to therapy resistance[85], and there are other examples[4,87]. This raises the possibility that drugs with senomimetic properties may warrant further consideration alongside more traditional senescence-inducing agents that could be combined with known senolytics/senomorphics to exploit this effect to improve overall anti-cancer treatment benefits.

Related to this, our study explores the dual effects of senescent cells as both promoters and suppressors of tumor immunosurveillance programs. Induced senescence induced by MEK and CDK4/6 TKIs can improve T-cell infiltration by altering the tumor vasculature[12] and promote tumoricidal activity of NK cells[13], while senescence induced in stromal and tumor cells can limit cytotoxic T-cell infiltration by recruiting suppressive myeloid cells[16,25] or upregulating surface markers capable of inactivating NK and T-cells[24]. In this study, we found similar opposing immune-modulating properties induced by VEGFR TKIs in tumor cells. This included direct suppression of CD8 T-cells activation *ex vivo* via secretory proteins (using the CM) and simultaneous reversal of this effect by surface proteins[90], suggesting that the overall activation of CD8 T-cells by SM+ tumor populations is the result underlying competing programs. These findings highlight the complexity of senomimetic tumor and immune cell interactions, including opposing extracellular proteomic programs impacting the immune microenvironment. Indeed, our finding that SM+ tumors grew faster in immune-deficient mice suggest that SM+ tumor cells interact with adaptive immune cells including CD8 T-cells to favor tumor control. This may explain why targeting immune-checkpoints with VEGFR TKIs might specifically block this SM+ subpopulation with greater effect. Notably, the immunogenic capability of SM+ isolated tumor cells has also been suggested in studies following treatment with doxorubicin[91] or irinotecan[92] and highlight the broad implications of the immune-priming ability of SM+ subpopulations for various cancer therapies and models.

In this regard, our results introduce a key role for STING and type I IFN signaling in both senescence and immune responses after VEGFR TKI treatment. Tumoral STING activation can improve responses to ICIs by increasing recruitment/infiltration of cytotoxic T-cells in multiple cancer models[35,93-95]. Similarly, type I IFNs can induce tumor immunogenicity by increasing antigen presentation and secretion of chemo/cytokines capable of attracting multiple immune cells[63]. For example, chemotherapy can induce IFN signaling in tumor cells and trigger an innate immune response that, in turn, promotes treatment response[96]. Thus far, the connection between

IFN signaling and VEGFR TKI:ICI efficacy has only been made with type II IFNγ. For example, Adachi and colleagues found that FGFR signaling in human and mouse kidney cancer cells limits tumoral IFNγ signaling, decreasing antigen-presentation and immune-checkpoint protein expression[97]. They then showed that lenvatinib - a multi-targeted VEGFR TKI with FGFR1-4 blocking activity – improved *in vivo* tumor responses with PD-1 targeting antibody by preventing this exogenously stimulated IFN signaling[97]. In our study, we identify STING pathway activation, and particularly the stimulation of Type I IFNs, as a broad collateral drug-class side-effect of VEGFR TKI treatment. We found VEGFR TKI triggered SM-expression that, in turn, stimulated surface-expressing ISGs such as MHC-I and PD-L1. Such results are similar to effects observed with CDK4/6 inhibitors, which also activate IFN signaling in tumor cell immunogenicity[98] and can also increase MHC-I expression[64]. These findings raise the question of whether underlying STING/IFN activating properties of VEGFR TKIs may be responsible for enhanced immunogenicity in tumors. In this regard, a recent study by Yang *et al* did identify a role for STING regulation in tumor blood vessel reprogramming (in endothelial cells) that could enhance VEGFR TKI/ICI combinatory effects by normalizing blood flow[99]. Our results introduce a novel *tumor-intrinsic* STING activation by VEGFR TKIs, raising the potential that selecting VEGFR TKIs based on the strength of STING activation may explain increased potency of select compounds in clinical testing with ICIs.

Since our studies used SA-β-gal activity to identify SM-expression, lysosome function and autophagy may impact immune-modulatory functions of tumor cells. β-galactosidase is a hydrolase enzyme located in lysosomes that catalyzes the hydrolysis of β-galactosides into monosaccharides[41]. SA-β-gal activity is used as surrogate for lysosomal pH changes (from ~4 to ~6[100]) and for increased lysosomal mass, both common attributes of senescent cells[101,102]. Yet the precise function of SA-β-gal in tumors remain unclear as it can contribute to senescent phenotype induction, maintenance and overall effector functions. For instance, chemotherapy and various TKIs can accumulate in the lysosomes of tumor cells[103,104] thereby increasing lysosomal mass, which has been linked to drug resistance[103-106]. Consistent with these findings, our results show that type I IFNs can regulate SA-β-gal, which is consistent with reports of IFNs regulating multiple facets of lysosomes, including sub-cellular localization, protein content, pH and protease activity[107]. It is possible that TKI-induced changes in type I IFNs are related to changes in lysosomal mass, which may reflect the relationship between SM+ cells and enhanced

IFN responses. This may explain the increased immunogenicity of SM+ cells and suggest lysosomal mass or function can directly impact ICI responses because of type I IFN release. Studies are currently underway to examine this hypothesis.

Outstanding questions raised by our study include a mechanism that could explain *how* VEGFR TKIs may activate the STING pathway, in particular whether this is a direct or indirect side-effect of this drug class. Overall STING expression was found to increase by VEGFR TKI treatment raising the possibility that programs regulating either STING production or degradation may be altered. Signals that lead to STING protein production may occur dependent or independent of cGAS[108], or STING degradation may be reduced by TKI-induced alterations in lysosomal functions[103,104]. Notably, a role for NFκB was not explored in this study but is a STING-activated protein induced (along with mTOR) by VEGFR TKIs that can control IFN/ISG expression along with SASPs [7,109-111]. While we have previously shown SM+ tumors can be more sensitive to NF-κB/mTOR signaling disruption, further study is needed to assess whether induced immune modulation in tumors would be enhanced or abrogated when NF-κB signaling is blocked during VEGFR TKI and αPD-L1 drug combinations. Finally, our results show that secreted factors from SM+ cells could suppress activation of T-cells. This raises a key question: Is it better or worse for treatments to enhance SM-expression in tumor cells? Elevation of SM+ cell populations in tumors by VEGFR TKI treatment may increase T-cell suppression induced by secretory factors, something that could nullify antitumor effects. Indeed, a recent study by Choi *et al* showed that secreted factors such as CXCL12 from senescent cells can limit the infiltration of T-cells and, by blocking CXCL12 with a neutralizing antibody, T-cell infiltration was improved[16]. Chronic IFN activation in tumor cells can also be a source of a T-cell suppressing secretome[112-114]. It is possible that certain secreted factors driven by type I IFN signaling in SM+ cells can suppress the activity of T-cells. It is also possible that identification of specific secreted factors produced by SM+ cells on T-cell suppression followed by therapeutic neutralization could improve the immune-priming effects of SM+ cells and VEGFR TKIs. Future studies will be needed to tease out specific secretory molecules resulting in T-cell suppression without inhibiting immune-stimulating molecules also fueled by IFN and STING.

Taken together, our results show that VEGFR TKIs can activate type I IFN and STING signaling in tumor cells resulting in IFN-enriched SM+ cell populations capable of both inhibiting and stimulating CD8 T-cell activity. Importantly, we found that SM+ tumor growth is

more sensitive to anti-PD-L1 inhibition, raising the possibility of exploiting STING-activating and senomimetic properties as a way to select optimal pairings of VEGFR TKIs for ICI combinations in the clinical setting.

Acknowledgements

We would like to thank K. Rathmell and V. Benjamin for guidance on use of published data; and thank A. Tracz, S.Tzetzo, and B.Chatterton, for their technical support. Biorender was used in image production.

Funding: This work used shared resources supported by the Roswell Park Comprehensive Cancer Center (RPCCC) Support Grant from the National Cancer Institute (NCI) (P30CA016056). This work was supported by grants to JMLE from the American Cancer Society (ACS) via a Research Scholar Grant (RSG-18-064-01-TBG) and a Mission Boost Grant (MBGI-23-1038434-01-MBG). Opinions, interpretations, conclusions and recommendations are those of the author and not necessarily endorsed by the NCI or ACS.

Author Contributions: Conceptualization, MD, JMLE; Methodology, MD, YS, CV, SB, JB, MM, JMLE; Investigation, MD, YS, AM, WH, CV, MM, JMLE; Formal Analysis, MD, YS, MM, ML, CV, AM, JMLE; Funding Acquisition, JMLE; Writing – Original draft, MD, JMLE; Writing – Review and Editing, MD, YS, AM, MM, JMLE.

Declaration of Interests: None

Materials and Methods

Cell lines

Cell lines used in this study include:

Mouse mammary carcinoma 4T1 cells were obtained from A. Gudkov, Roswell Park Comprehensive Cancer Center, RPCCC and described previously[115]. Mouse mammary carcinoma EMT6 cells used in this study were obtained after a period of *in vivo* tumor growth (described elsewhere as EMT6-$P^{vivo\ 113}$). Human breast carcinoma LM2-4 cells (a metastatic derivative of MDA-MD-231) and mouse kidney carcinoma RENCA cells express luciferase and have been described elsewhere as LM2-4^{LUC+} and $RENCA^{LUC+}$, respectively[116-118]. Cells were maintained in RPMI (Corning cellgro; 10-040-CV for 4T1, EMT6, and RENCA) or DMEM (Corning cellgro; 10-013-CV for LM2-4). Growth media were supplemented with 5% v/v FBS (Corning cellgro; 35-010-CV or Gibco; 10437028). Cells were maintained at 37°C with 5% CO_2 in a humidified incubator. Human cells were authenticated by STR profile comparison to ATCC cell database and mouse cells were confirmed of species origin (DDC Medical, USA).

Mouse tumor models

Study approval

Animal studies were performed in strict accordance with the recommendations in the Guide for Care and Use of Laboratory Animals of the National Institutes of Health and according to guidelines of the Institutional Animal Care and Use Committee (IACUC) at Roswell Park Comprehensive Cancer Center (RPCCC). All studies were approved by the IACUC at RPCCC according to Protocol 1227M. All personnel involved in this study were included in the IACUC protocol and approved/trained by veterinary staff to conduct all experimental procedures described.

Orthotopic Tumor Implantations

$4T1^{P}$, $4T1^{AxR}$, $4T1^{AxR}$ SM+, and $4T1^{AxR}$ SM- ($4x10^4$ cells in 100uL RPMI), $EMT6^{P}$ ($5x10^5$ cells in 100 µL RPMI), $EMT6^{CaR}$ SM+, $EMT6^{CaR}$ SM- ($1.5x10^5$ cells in 100uL RPMI), were implanted orthotopically into the right inguinal mammary fat pad in 6-12 week-old female

Balb/c or SCID mice. Isoflurane (anesthesia) and buprenorphine (analgesic) were used during all surgical implantations. Mammary tumors were measured using Vernier calipers and volumes were calculated using the formula ($width^2$ x length) x 0.5. All animals were assessed 2-3 times daily by veterinary staff or personnel approved by IACUC for pre-defined endpoints.

Derivation and maintenance of TKI-resistant cells:

The generation of 4T1 Axitinib-resistant ($4T1^{AxR}$) cells have been described previously[7,115]. Briefly, 4T1 cells were orthotopically implanted into Balb/c mice. Mice were treated with Ax (100mg/kg/day) during primary tumor growth and, following surgical removal of the primary tumor, treatment was continued until mice reached a metastasis-related endpoint or study endpoint. At endpoint, spontaneous metastatic lesions were excised from lung, dissociated, and then adapted to cell culture containing 0.5μM Ax treatment until experimental use. $4T1^{AxR}$ cells were compared with *in vitro*-maintained parental 4T1 ($4T1^{P}$) in this manuscript. For the generation of *in vivo*-derived EMT6 cabozantinib-resistant ($EMT6^{CaR}$) cells, Balb/c mice were orthotopically implanted with EMT6 cells and then treated continuously with Ca (30mg/kg/day) until endpoint based on primary tumor size limits. An EMT6 metastatic variant ($EMT6^{M}$) was obtained from vehicle treated mice and used as a control for $EMT6^{CaR}$ cells. At endpoint $EMT6^{CaR}$ and $EMT6^{M}$ variants were selected from metastatic lesions in lungs which were minced and then placed in RPMI media (supplemented with 5% v/v FBS, 100IU/ml penicillin and 1000ug/ml streptomycin) with DMSO for $EMT6^{M}$ or with Ca (2μM) for $EMT6^{CaR}$. One week later, antibiotics were removed, and the highest tolerated concentration of Ca (2μM) was continued *in vitro* for $EMT6^{CaR}$ cells. $EMT6^{M}$ cells were maintained in the equivalent volume of DMSO.

Fluorescent live-cell assay and isolation of SA-βgal-based SM+ and SM- expressing cells

Cells were grown in corresponding media and at approximately 90% confluency, media containing 100nM Bafilomycin A1 (SCBT, sc-201550A) was placed on cells for 1 hour (to alkalinize the lysosomes to increase pH for optimal detection of SA-β-gal). C_{12}FDG (Setareh Biotech, 7188) a fluorogenic substrate for β-gal was then added for 1 hour at a final concentration of 33μM as previously described[8,28,42]. Cells were then washed 2x with PBS, trypsinized, and prepared for processing with a LSR II flow cytometer for SA-β-gal

quantification or FACS Aria cell sorter (Becton Dickinson) for studies involving TKI-treatments, AxR or CaR variant isolation into SM+ ($C_{12}FDG^{Hi/+}$) and SM- ($C_{12}FDG^{Lo/-}$) cell populations (**Appendix 1 shows experimental schematic and gating strategy**). Isolated fractions were either processed immediately or maintained with drug exposure for experiment duration (as in Fig 1C). For isolated fractions implanted orthotopically in vivo shown in Figure 5A, each condition shown represent separate studies with separate days for sorting SM+/SM- cell populations. Due to variations in the sorting process and time taken to amass sufficient cells for implantation, these experiments were performed separately and allow for *inter*-experiment comparisons (i.e., SM+ vs SM- in one condition) but not *intra*-experimental comparisons (i.e., SM+ vs SM+ in separate conditions). For *ex vivo* evaluation of SM expression following VEGFR TKI 48-hour treatment, tumors were minced with forceps into 2-4mm pieces and digested with 1x Collagenase/Hyaluronidase (STEMCELL, 07919) in RPMI + 5% FBS for 1 hour shaking at 37°C. Isolated cells were treated with RBC lysis buffer (Biolegend, 420302), washed with PBS, and plated for $C_{12}FDG$ staining as described above. Following $C_{12}FDG$ staining, cells were washed, trypsinized and spun down at 1500rpm for 5 minutes, stained with Zombie Aqua Fixable Viability Kit (Biolegend, 423102), and then stained with CD45-Ax700 (Biolegend, 147715) according to manufacturer instructions. Cells were then washed with Cell staining buffer and analyzed on LSRII flow cytometer. Data was analyzed with FCS Express 7 (De Novo Software).

Identification of SM+ and SM- cell signatures

To identify a gene signature specific to SM+ or SM- cell populations, we compared $4T1^{AxR}$ SM+ vs. $4T1^{P}$ or $4T1^{AxR}$ SM- vs. $4T1^{P}$ bulk transcriptomic data and extracted upregulated genes with a fold-change >1.5 and an adjusted p-value <0.05 for each respective cell population. Next, from these upregulated genes we subsetted to genes upregulated in $4T1^{AxR}$ SM+ vs. $4T1^{AxR}$ SM- to obtain a SM+ gene signature. Then we subsetted genes upregulated in $4T1^{AxR}$ SM- vs. $4T1^{AxR}$ SM+ to obtain a SM- gene signature and included genes with a fold-change > 1.5 and an adjusted p-value <0.05 (see **Supplementary Table S2 for gene names for SM+/SM- populations and gene signatures**).

Generation of an SM+ T Score

To generate SM+ T-scores to rank expression of SM+/SM- gene signatures in gene expression datasets, a t-statistic (or T-score) was obtained by comparing the expression of the SM+ signature genes to SM- signature genes for each sample using a t-test statistical comparison[119]. SM+ T-scores were obtained for each sample and reported as a single scalar score. A higher SM+ T-score signifies a higher proportion of SM+ genes or a lower proportion of SM- genes, while a lower SM+ T-score signifies a lower proportion of SM+ genes or a higher proportion of SM- genes. An example Rscript code is as follows:

```
SM+ score <- apply(scale(gene expression matrix), 2, function(x){
t.test(x[rownames(gene expression matrix) %in% SM+ gene signature],
x[rownames(gene expression matrix) %in% SM- gene signature])$stat.
```

Validation of SM+ T-score and IFN enrichment in published datasets.

Publicly available clinical and preclinical data derived from studies involving VEGFR TKI treatment were obtained from the Gene Expression Omnibus (GEO, www.ncbi.nlm.nih.gov/geo/) or database of Genotypes and Phenotypes (dbGaP, https://www.ncbi.nlm.nih.gov/gap/).

Wood *et al*, 2020 (phs002053.v1.p1): In this study, pre-treatment and post-treatment biopsies were obtained from clear cell RCC patients treated with neoadjuvant pazopanib for 8-12 weeks for RNA-seq analysis (Illumina HiSeq2500) from pulverized frozen tissue[54]. Raw data were downloaded from the dbGaP database under protocol phs002053.v1.p1. Data were processed and normalized using the RNA-seq pipeline as described above, with the exception that reads were aligned to the human genome GRCH38 H27(gencode). Normalized gene counts were used to obtain SM+ T-scores, and differentially expressed genes set by a fold-change > 1.5 and an adjusted p-value of 0.05, were used to generate ranked gene lists for GSEA.

Braga *et al*, 2017 (GSE58837): In this study, pre-treatment and post-treatment tumor biopsies were obtained from locally advanced breast cancer patients receiving neoadjuvant Sunitinib for Affymetrix microarray whole transcriptome analysis of RNA collected from frozen tissue[55]. Processed and normalized microarray data were obtained from GEO and used to generate SM+ T-scores and for GSEA.

Diaz-Montero *et al*, 2016 (GSE76068): In this study, human specific normalized microarray data derived from tumors were obtained from GEO with accession number

GSE76068[56]. Specifically, a RCC patient sample was subcutaneously implanted into NOD-scid-IL2r$^{-/-}$(NSG) mice and treated with 40mg/kg/day Su. Tumor samples were collected before treatment and after treatment and analyzed using Illumina human expression BeadChips. Processed and normalized microarray data were obtained from GEO and used for GSEA.

Mastri *et al*, 2018 (GSE122819): LM2-4^{SuR} cell derivation has been described by us previously[7]. Briefly, whole transcriptomic profiling of LM2-4^{P} and LM2-4^{SuR} cells used Illumina human expression BeadChips. Normalized microarray expression data were obtained from GEO and used for GSEA.

Mathematical Modeling (Reduced Gompertz modeling):

Tumor growth kinetics was modeled using the reduced Gompertz model, which allows growth quantification and comparison between tumor growth curves. It defines a unique subject-specific growth parameter 'β', corresponding to the exponential decrease of the specific tumor growth rate, and a population-level parameter k [65]. This structural reduced Gompertz model was then embedded into a nonlinear mixed-effects statistical framework (population approach) that allows for the simultaneous modeling of tumor dynamics and inter-animal variability (described in Appendix 4) [65]. For each pair of groups to be compared, the reduced Gompertz model considered the population parameter k to have fixed effects within the population, while β was assumed to have both fixed and random effects. In this way, k (one fixed parameter) and β (one individual parameter) describes the total tumor volume V as function of time t:

$$\frac{dV}{dt} = \left(k\beta - \beta \ln\left(\frac{V}{V_0}\right)\right)V, \quad V(0) = V_0,$$

where V_0 is the volume of injected tumor cells. Tumor growth analysis to compare groups used Monolix2018R2 software and a combined error model was used. The two population parameters were estimated by maximizing the population likelihood, obtained by pooling together the data of each pair of groups. Finally, individual parameters were obtained by means of the empirical Bayes estimates. All parameters were well identified, and diagnostic plots such as the visual predictive check and residuals were compared to confirm descriptive performances of the reduced Gompertz model. This methodology allowed to estimate only one individual parameter β and to compare the distributions of this parameter in each pair of groups. A t-test was used to determine whether the mean of the estimated individual parameter β was the same for the two

groups. If the calculated p-value was found lower than 0.05, then the hypothesis that the distributions of β of the two groups were equal was rejected (**Appendix 4A-4D shows an example workflow of mathematical modeling used**).

The following additional Methods are included in Supplementary files:

- Gene knock-down using shRNA
- Drug and recombinant protein concentrations
- T-cell depletion studies
- Splenocyte division and Activation assays
- Flow cytometry analysis of cell surface proteins
- Cell proliferation assay
- RNA isolation
- qRT-PCR
- Western Blot Analysis
- RNA-sequencing analysis
- Gene set enrichment analysis (GSEA)
- Gene Ontology (GO) Enrichment Analysis
- Inteferome Analysis
- Quantification and Statistical Analysis

Data Availability

Publicly available clinical and preclinical data obtained from the Gene Expression Omnibus (GEO, www.ncbi.nlm.nih.gov/geo/) include GSE132568, GSE58837; GSE76068, and GSE122819. Clinical data were obtained from the database of Genotypes and Phenotypes (dbGaP, https://www.ncbi.nlm.nih.gov/gap/) with permission under protocol phs002053.v1.p1. Expression profile data generated an analyzed in this study were deposited to the NCBI GEO database GEO under accession number GSE226243. Additional details are provided in the Methods. All other data generated by the authors is available on request.

STAR★Methods

Key resources table

REAGENT or RESOURCE	SOURCE	IDENTIFIER
Antibodies		
Goat anti-rabbit IgG (H+L); HRP conjugated	Promega	Cat#W4011; RRID: AB_430833
Goat anti-mouse IgG(H+L); HRP conjugated	Promega	Cat#W4021; RRID: AB_430834
Rabbit Monoclonal Phospho-STING (S365) (D8F4W)	Cell Signaling	Cat#72971; RRID: AB_2799831
Rabbit Monoclonal STING (D1V5L) Rodent Preferred	Cell Signaling	Cat#50494; RRID: AB_2799375
XP Rabbit Monoclonal Phospho-TBK1/NAK-(S172) (D52C2)	Cell Signaling	Cat#5483; RRID: AB_10693472
Rabbit Monoclonal TBK1/NAK (D1B4)	Cell Signaling	Cat#3504; RRID: AB_2255663
Rabbit Monoclonal cGAS (D3O8O) Mouse Specific	Cell Signaling	Cat#31659; RRID: AB_2799008
Mouse Monoclonal Anti-alpha-tubulin Clone B-5-1-2	Sigma Aldrich	Cat#T6074; RRID: AB_477582
Purified anti-mouse CD3 antibody (Clone 17A2)	Biolegend	Cat#100202; RRID: AB_312659
Purified anti-mouse CD28 antibody (Clone 37.51)	Biolegend	Cat#102102; RRID: AB_312867
Anti-mouse CD45 antibody; Alexa Fluor 700 conjugated (Clone 30-F11)	Biolegend	Cat#103105; RRID: AB_312970
Anti-mouse CD8b.2 antibody; PE-Cy7 conjugated (Clone 53-5.8)	Biolegend	Cat#103128; RRID: AB_493715

Anti-mouse CD69 antibody; APC conjugated (Clone H1.2F3)	Biolegend	Cat#140416; RRID: AB_2564385
Anti-human/mouse Granzyme B antibody; Pacific Blue conjugated (Clone GB11)	Biolegend	Cat#515408; RRID: AB_2562196
Anti-mouse PD-L1 antibody (Clone 80)	Astra Zeneca (MTA)	N/A
Anti-mouse CD16/CD32 TruStain FcX	Biolegend	Cat# 101319; RRID: AB_1574973
Anti-mouse CD8a antibody; Alexa Fluor 488 conjugated (Clone 53-6.7)	Biolegend	Cat#: 100726; RRID: AB_493423
Anti-mouse CD8a antibody (Clone 2.43)	BioXCell	Cat#: BE0061; RRID: AB_1125541
Anti-mouse PD-L1 antibody; PE conjugated (Clone 10F.9G2)	Biolegend	Cat# : 124307; RRID: AB_2073557
Anti-mouse MHC-I (H-2kb/H-2Db/H-2Dd); APC conjugated (Clone 28-8-6)	Biolegend	Cat#: 114613; RRID: AB_2750193
Anti-mouse CD3 antibody; APC conjugated (Clone17A2)	Biolegend	Cat#:100235 ; RRID: AB_2561456
Bacterial and virus strains		
Biological samples		
Chemicals, peptides, and recombinant proteins		
Bafilomycin A1	Santa Cruz Biotechnology	Cat# sc-201550A; CAS: 88899-55-2
5-dodecanoylaminofluorescein di-β-D-galactopyranoside (C_{12}FDG)	Setareh Biotech	Cat#7188; CAS: 138777-25-0

Axitinib	Pfizer (MTA)	CAS: 319460-85-0
Cabozantinib	LC labs	Cat#: C-8901; CAS: 849217-68-1
Sunitinib malate	Pfizer (MTA)	CAS: 341031-54-7
Pazopanib	LC labs	Cat#P-6706; CAS: 444731-52-6
Lenvatinib	LC labs	Cat: L-5400; CAS: 417716-92-8
Tivozanib	Selleck Chem	Cat: S1207; CAS: 475108-18-0
SN-011	MedchemExpress	Cat: HY-145010
DMXAA	Selleck Chem	Cat: S1537; CAS: 117570-53-3
MSA-2	R&D systems	Cat: 7353/10 CAS: 129425-81-6
Recombinant mouse Interferon-alpha-2	Sino Biological	Cat#50525-MNAY; AS# NP_034633.2
Recombinant mouse interferon-beta	Sino Biological	Cat#:50708-MCCH; AS#: P01575
Recombinant mouse interferon-gamma	Peprotech	Cat#: 315-05; CAS:
RPMI	Corning	Cat#: 10-040-CV
DMEM	Corning	Cat#: 10-013-CV
Heat Inactivated-FBS	Gibco	Cat#: 10437028
Heat Inactivated FBS	Corning	Cat#: 35-010-CV
Trypsin	Corning	Cat#: 25-053-CI
Beta-mercaptoethanol	Gibco	Cat#: 21985023
Non-essential amino acids	Gibco	Cat#: 11140050
Sodium Pyruvate	Gibco	Cat#: 11360070
Penicillin/Streptomycin	Corning	Cat#:30-001-CI
RBC lysis buffer	Biolegend	Cat#: 420301

CFSE	Biolegend	Cat#: 423801
Zombie Aqua Fixable Viability Kit	Biolegend	Cat#: 423102
Activation cocktail + Brefeldin A1	Biolegend	Cat#: 423303
Accutase	Biolegend	Cat#: 423201
Critical commercial assays		
Qiagen RNA Mini Isolation Kit	Qiagen	Cat#74104
CellTiter 96 Aqueous Non-Radioactive cell proliferation kit (MTS)	Promega	Cat# G1112
Deposited data		
Expression data from breast cancer tumors treated with a single window of the VEGFR TKI sunitinib	Braga *et al*. 2017	GEO: GSE58837
Gene expression changes in human breast cancer cells (LM2-4) after sunitinib resistance	Mastri *et al*., 2018	GEO: GSE122819
Gene expression changes in mouse breast cancer cells (4T1) resistant to axitinib derived in vivo after continuous axitinib treatment from post-surgical metastatic lesions and then maintained in vitro with 0.5uM axitinib for more than 2 months.	Dolan and Mastri *et al*., 2019	GEO: GSE132568
Gene expression data from human clear cell renal cell carcinoma tumors treated neoadjuvantly with pazopanib for 8-12 weeks.	Wood *et al*., 2020	dbGaP: phs002053.v1.p1
Gene expression data from changes in renal cell carcinoma patient derived xenografts treated with the VEGFR TKI sunitinib	Diaz-Montero *et al*., 2016	GEO:GSE76068
Gene expression data from FACS isolated $4T1^{AxR}$ SM+ ($C_{12}FDG^{Hi/+}$) and SM- ($C_{12}FDG^{Lo/-}$) tumor cells	This paper	GEO: GSE226243
Experimental models: Cell lines		
4T1	Laboratory of A. Gudkov	
$4T1^{AxR}$	Mastri *et al*., 2018	
EMT6	Laboratory of A. Gudkov	
$EMT6^{CaR}$	This paper	
$EMT6^{M}$	This paper	
LM2-4	Laboratory of R. Kerbel	
RENCA	Laboratory of R. Pili	

$4T1^{shCon}$	This paper	
$4T1^{STING-KD}$	This paper	
$EMT6^{shCon}$	Shi *et al*., 2021	
$EMT6^{IFNAR1-KD}$	Shi *et al*., 2021	
Experimental models: Organisms/strains		
SCID mouse	Roswell Park Comprehensive Cancer Center	
Balb/cAnNCrl mouse	Charles River Labs	
Oligonucleotides		
Primers for qRT-PCR, see table S3	This paper; Integrated DNA Technology (IDT)	N/A
Recombinant DNA		
STING shRNA: ATGATTCTACTATCGTCTTAT	Sigma Aldrich	Cat#: TCRN000346320
IFNAR1 shRNA: GCCAGAGACTACTTACTGTTT	Shi *et al*., 2021	
Software and algorithms		
FCS Express 7 De Novo Software		N/A
FACSDiva Software	BD Biosciences	N/A
Graphpad		
R v.4.3.1	The Comprehensive R Archive Network	N/A
RStudio v.1.2.5033	Integrated Development for R/Posit	N/A
Limma v.3.56.2		https://bioconductor.org/packages/release/bioc/html/limma.html
EdgeR v.3.17		
Gene Set Enrichment Analysis (GSEA)	Broad Institute	https://www.gsea-msigdb.org/gsea
Gene Ontology Enrichment Analysis (GO)	Gene Ontology Consortium	https://geneontology.org

Interferome v2.01		http://www.interferome.org/interferome/home.jspx
Image Lab™ v6.0.1 build 34	Bio-Rad	
Image Lab ™ Touch Software v.2.4.0.03	Bio-Rad	
CFX Maestro	Bio-Rad	https://www.bio-rad.com/en-us/product/cfx-maestro-software-for-cfx-real-time-pcr-instruments?ID=OKZP7E15
xMark Microplate Spectrophotometer MPM6.exe v6.3	Bio-Rad	
NanoDrop 2000/2000c v1.6.198	Thermo Fisher Scientific	
Other		
iScript cDNA synthesis kit		
iTaq DNA polymerase	Bio-rad	Cat# 1725120
FCS Express 7 De Novo Software		N/A
FACSDiva Software	BD Biosciences	N/A

Figure Legends

Fig 1: Enriched IFN signaling in SM+ tumor cells after VEGFR TKI treatment

(**A**) Schematic showing isolation of tumor cells expressing the senescence-marker (SM) SA-β-gal after axitinib (Ax) treatment *in vivo* (Resistant, R) or *in vitro* (Short term, ST). R cell derivation described previously[7], see Methods.

(**B**) Representative FACS image of high- and low-expressing SM cells (SM+ or SM-) using C_{12}FDG staining in $4T1^{AxST}$ cells.

(**C**) After FACS isolation, $4T1^{AxR}$ SM+ and SM- cells were assessed for proliferation daily by MTS assay, and cell viability tested by trypan blue staining (inset; Day 0). n=3.

(**D**) Schematic showing RNA-sequencing of FACs isolated $4T1^{AxR}$ SM+ and SM- cells cell populations based upon SM cell expression and differential gene expression.

(**E**) Volcano plot representing differentially expressed genes (Log_2 [Fold Change] ≤ -1.5 or ≥ 1.5 and FDR ≤ 0.05) in $4T1^{AxR}$ SM+ (left; red) and in $4T1^{AxR}$ SM- (right; blue) compared to 4T1 cells. Venn diagram summarizing unique and shared differentially expressed genes between SM+/SM- cells compared to 4T1 cells.

(**F**) Cytoscape visualized GO analysis of significantly over-represented biological processes unique to the $4T1^{AxR}$ SM+ cells.

(**G**) GSEA of $4T1^{AxR}$ SM+ (compared to $4T1^{AxR}$ SM-) shown by a lollipop plot representing NES of curated or published senescence or therapy-induced secretome gene sets (blue), immunity/immune response gene sets (red), or shared between senescence and immune responses (red and blue overlap). *Note: Gene set information is summarized in Table S1.*

(**H**) Hallmark GSEA of $4T1^{AxR}$ (compared to $4T1^{P}$) and $4T1^{AxR}$ SM+ (compared to $4T1^{AxR}$ SM-). All gene sets selected had an FDR < 0.05. IFN response genesets shown in black.

(**I**) Volcano plot representing differentially expressed genes in $4T1^{AxR}$ SM+ cells (compared to $4T1^{AxR}$ SM-). DEGs were then used in an interferome analysis to determine the relative percentage of DEGs regulated by IFNs.

(**J-M**) Gene Expression of select ISGs evaluated by qRT-PCR were compared in the following cells;

(J) $4T1^{AxR}$ vs. $4T1^{P}$ cells (n=3).

(K) SM+ vs. SM- populations derived from $4T1^{AxR}$ cells after C_{12}FDG FACS-isolation (n = 3-6)

(L) 4T1 vs. 4T1+Ax (ST with Ax) cells (n = 3)

(M) SM+ vs. SM- populations derived from 4T1+Ax cells after C_{12}FDG FACS-isolation (n = 3)

(**N**) SM-expression in 4T1 tumor cells following ST treatment with VEGFR TKIs Ax, Ca, Tivo, Pazo, or Len analyzed by flow cytometry.

Axitinib-Resistant (AxR) Axitinib (Ax); Vascular Endothelial growth factor receptor (VEGFR); Tyrosine Kinase Inhibitor (TKI); Short-term (ST); ST Ax-treated (+Ax); Fluorescent-activated cell sorting (FACS); Senescence-associated (SA); beta-galactosidase (β-gal); 5-Dodecanoylaminofluorescein Di-β-D-Galactopyranoside (C_{12}FDG); Senescence-Marker (SM); High-Expressing (SM+); Low-Expressing (SM-); Fold-Change (FC); Differentially Expressed Genes (DEGs); False Discovery Rate (FDR); Gene Ontology (GO); Gene Set Enrichment Analysis (GSEA); Normalized Enrichment Score (NES); Interferon-stimulated gene (ISG); In vivo-derived Parental (P); Vehicle control (Veh.); Cabozantinib (Ca); Tivozanib (Tivo);

*Pazopanib (Pazo); Lenvatinib (Len); Quantitative data shown as mean ± SD. * p <0.05; ** p < 0.01; *** p < 0.001; **** p < 0.0001.*

Figure 2: An IFN-enriched SM+ T- score increases after TKI treatment

(**A-D**) Comparisons of GSEA of hallmark IFNα and IFNγ response gene sets in published studies involving VEGFR TKIs before treatment (pre-Tx) and after treatment (post-Tx).

(**A**) Neoadjuvant Pazo-treated ccRCC patients (dbGaP #phs002053.v1.p1; n = 5-17; bulk RNA-seq)

(**B**) Neoadjuvant Su-treated locally advanced BC patients (GEO:GSE58837; n = 5-7 ; bulk RNA-seq)

(**C**) Su-treated human RCC PDX model (GEO:GSE76068; n = 4; microarray)

(**D**) Su-treated human metastatic BC tumor cell line (GEO:GSE122819; n = 3 ; microarray)

(**E**) Schematic of SM+ T-score generation using gene signatures from $4T1^{AxR}$ SM+ and SM- cells.

(**F-I**) SM+ T-score analysis in neoadjuvant TKI-treated patients.

(**F**) SM+ T-score in matched pre- and post-treatment samples from ccRCC patients (n = 5).

(**G**) SM+ T-score in post-treatment samples (ccRCC; n = 17).

(**H**) SM+ T-score in matched pre- and post-treatment samples from BC patients (n = 4).

(**I**) SM+ T-score in post-treatment samples (BC; n = 5).

Parental (P); Clear Cell Renal cell carcinoma (ccRCC); Breast Cancer (BC); Senescence-Marker (SM); High-Expressing (SM+); Low-Expressing (SM-); Fold-Change (FC); False Discovery Rate (FDR); Patient-derived xenograft (PDX); Gene Expression Omnibus (GEO); GEO Series records (GSE); database of Genotypes and Phenotypes (dbGaP); Gene Set Enrichment Analysis (GSEA); Normalized Enrichment Score (NES); Sunitinib (Su); Pazopanib (Pazo)

Figure 3: SM expression can be regulated by a STING-IFNβ signaling axis

(**A**) Protein expression of the STING pathway including pSTING, STING, pTBK1, TBK1, and alpha-tubulin in $4T1^{P}$ and $4T1^{AxR}$ tumor cells (n=3).

(**B**) Densitometry quantification of western blots shown in (Fig 3A) representing Log_2FC in relative pSTING (top), pTBK1 levels (middle), and STING levels (bottom) compared to P controls. Expression is normalized to α-tubulin (n=3).

(**C**) SM-expression in 4T1 tumor cells following treatment with DMXAA or MSA-2 analyzed by flow cytometry (n=3).

(**D**) Protein expression of the STING pathway in 4T1 tumor cells following treatment with vehicle control, STING agonists (MSA-2, DMXAA), or multiple VEGFR TKIs (Ax, Ca, Su, Tivo, Pazo, Len) (n=3).

(**E**) Densitometry quantification of western blots shown in (D) representing Log_2FC in relative pSTING (top), pTBK1 levels (middle), and STING levels (bottom) compared to vehicle controls. Expression is normalized to α-tubulin (n=3).

(**F**) Protein expression of STING pathway in $4T1^{shCon}$ or $4T1^{STING\text{-}KD}$ cells following Ax treatment analyzed by western blotting (n=2-3)

(**G**) Gene expression of select ISGs evaluated by qRT-PCR in $4T1^{shCon}$ or $4T1^{STING\text{-}KD}$ tumor cells following Ax treatment (n=3).

(**H**) SM-expression in $4T1^{shCon}$ or $4T1^{STING\text{-}KD}$ tumor cells following Ax treatment analyzed by flow cytometry (n=3).
(**I**) SM-expression in $EMT6^{M}$ and $EMT6^{CaR}$ cells following SN-011 treatment analyzed by flow cytometry (n=3).
(**J**) Protein expression of the STING pathway including pSTING, STING, pTBK1, TBK1, and alpha-tubulin in $EMT6^{M}$ and $EMT6^{CaR}$ tumor cells (n=3).
(**K**) Densitometry quantification of western blots shown in (Fig 3J) representing Log_2FC in relative pSTING/STING (top) and pTBK1/TBK1 levels (bottom), compared to M controls. Expression is normalized to α-tubulin (n=3).
(**L**) SM-expression in 4T1 tumor cells following stimulation with IFNα, IFNβ, or IFNγ analyzed by flow cytometry (n=3)
(**M**) Gene expression of Ifnα, Ifnβ, or Ifnγ genes in 4T1 tumor cells following Ax treatment evaluated by qRT-PCR (n=3).
(**N**) Gene expression of Ifnβ in $4T1^{shCon}$ or $4T1^{STING\text{-}KD}$ tumor cells following Ax treatment evaluated by qRT-PCR (n=3).
(**O**) SM-expression in $EMT6^{shCon}$ or $EMT6^{IFNAR1\text{-}KD}$ cells following Ax or Ca treatment evaluated by flow cytometry (n=3).
*Axitinib (Ax); Cabozantinib (Ca); Sunitinib (Su); Pazopanib (Pazo); Tivozanib (Tivo); Lenvatinib (Len); shRNA Vector Control (shCon); Vehicle control (Veh); 5-Dodecanoylaminofluorescein Di-β-D-Galactopyranoside (C_{12}FDG); Interferon (IFN); Short-term (ST); Fold Change (FC); Type I IFN receptor knockdown (IFNAR1-KD); Stimulator of Interferon Genes knockdown (STING-KD); 5,6-dimethylxanthenone-4acetic acid (DMXAA); cells were treated with 10ng/ml of IFNs or TKIs for 48 hours (A); Drug concentrations included SN-011 (6-8μM), (DMXAA (50μM), MSA-2 (33μM), Ax (0.5μM), Ca (2μM), Su (2μM), Tivo (2μM), Pazo (2μM), or Len (2μM). Quantitative data is shown as mean ± SD; * p <0.05, ** p<0.01, *** p < 0.001, **** p<0.0001*

Figure 4: SM+ cells express opposing regulators of immunity
(A-D) Evaluation of antigen presentation molecules by qRT-PCR included the following comparisons:
(A) 4T1 cells after Veh or Ax treatment (n=3)
(B) $4T1^{shCon}$ or $4T1^{STING\text{-}KD}$ cells after Veh or Ax treatment (n=3).
(C) $4T1^{AxR}$ compared to $4T1^{P}$ (n=3).
(D) FACS-isolated $4T1^{AxR}$ SM+ cells compared to $4T1^{AxR}$ SM- cells (n=3-6).
(E) Cell surface MHC-I expression in 4T1 cells after Ax or Ca treatment. Representative histogram (left; Ax only) and quantification by flow cytometry (right; n=3).
(F) Cell surface PD-L1 expression in 4T1 cells after Ax or Ca treatment. Representative histogram (left; Ax only) and quantification by flow cytometry (right; n=3).
(G) Representative histograms of staining and gating used to evaluate MHC-I and PD-L1 surface expression on 4T1 SM+/SM- cell populations after Ax treatment.
(H) Quantification of MHC-I in SM+/SM- gated cell populations in 4T1 cells after Ax or Ca treatment by flow cytometry (n=3).
(I) Quantification of PD-L1 in SM+/SM- gated cell populations in 4T1 cells after Ax or Ca treatment by flow cytometry (n=3).

*Axitinib (Ax); Cabozantinib (Ca); shRNA Vector control (shCon); Vehicle (Veh); 5-Dodecanoylaminofluorescein Di-β-D-Galactopyranoside (C_{12}FDG); Interferon (IFN); Short-term (ST); Median Fluorescence Intensity (MFI); Fold Change (FC); Stimulator of Interferon Genes (STING); STING knockdown (STING-KD). Dotted line in A-D shows average value of vehicle (Veh.) treated or parental controls. Quantitative data is shown as mean ± SD; * p <0.05, ** p<0.01, *** p < 0.001, **** p<0.0001*

Figure 5: Contact-*dependent* CD8 T-cell stimulation by SM+ cells can off-set contact-*independent* CD8 T-cell inhibition.

(A) Primary tumor growth following orthotopic implantation of FACS enriched $4T1^{AxR}$ SM+ and $4T1^{AxR}$ SM- tumor cells in BALB/c mice (left, representative example, n = 5), SCID mice (n = 5, middle), and BALB/c mice treated with an anti-CD8 antibody (right, n = 10).

(B) Summary of difference in the Gompertz model parameter β (specific growth rate increase) from growth kinetics analysis of primary tumor growth curves in (A). (BALB/c mice, n = 34 (4 independent experiments); SCID mice, n = 5; BALB/c treated with anti-CD8 antibody, n = 10).

(C) Schematic of BALB/c derived splenocytes treated with CM derived from $4T1^{P}$ or $4T1^{AxR}$ tumor cells or co-cultured with $4T1^{P}$ or $4T1^{AxR}$ tumor cells.

(**D-E)** Log_2FC of %Divided, %GRMB+, or %IFNy+ gated CD8+ splenocytes following (D) treatment with CM derived from $4T1^{AxR}$ tumor cells compared to $4T1^{P}$ or (E) co-cultured with $4T1^{AxR}$ tumor cells compared to $4T1^{P}$.

(F) Schematic of Balb/c derived splenocytes treated with CM derived from SM+ or SM- tumor cells or splenocytes co-cultured together with SM+ or SM- cell populations.

(G-H) Log_2FC of % Divided, % GRMB+, or % IFNγ+ gated CD8+ stimulated splenocytes following (G) treatment with CM derived from $4T1^{AxR}$ SM+ tumor cells compared to SM- cells or (H) co-cultured with $4T1^{AxR}$ SM+ tumor cells compared to SM- tumor cells.

(I-J) Heatmap summarizing Log_2FC of % Divided, %GRMB+, %IFNγ+ CD8+ gated stimulated splenocytes for CM or co-cultures comparing (I) $4T1^{AxR}$ vs. P controls and $EMT6^{CaR}$ vs. P controls or (J) $4T1^{AxR}$ SM+ vs. SM- and $EMT6^{CaR}$ SM+ vs. SM- controls.

(I) Graphical summary of opposing effects of SM-expressing tumor cells on CD8 T-cell activity.

*Parental (P); Axitinib-resistant (AxR); Senescence-marker (SM); 5-Dodecanoylaminofluorescein Di-β-D-Galactopyranoside (C_{12}FDG); Senescence-marker (SM); Granzyme B (GRMB); Interferon-gamma (IFNγ); Conditioned media (CM); Forward Scatter (FCS); Fold Change (FC); Primary tumor burden was assessed by caliper measurement. See Appendix 3 for details of reduced Gompertz and mixed-effects modeling to evaluate tumor growth kinetics. Graphs in D, E, G, H show Log2FC comparisons from controls standardized to '0' (grey circles and error bars shown). Standard deviation (SD); Quantitative data is shown as mean ± SD; * p <0.05, ** p<0.01, *** p < 0.001, **** p < 0.0001.*

Figure 6: SM+ tumors have increased sensitivity to PD-L1 inhibition

(A) Schematic and quantification of % SM-expressing viable and CD45- gated cells isolated from tumors in Balb/c mice orthotopically implanted with 4T1 tumor cells and treated with Ax for 48 hours in established tumors (~400m^3).
(B) Primary tumor growth of Balb/c mice orthotopically implanted with 4T1 tumor cells and treated with Veh control, Ax, anti-PD-L1, or Ax + anti-PD-L1 once tumors reached 400mm^3 (n = 5)
(C) FC comparison of primary tumor growth from (B) from endpoint to start of treatment (DPI 17).
(D) Difference in tumor growth rate using Gompertz modeling (upper) and area under the curve (AUC) analysis of primary tumor growth curves (B) after DPI 17 until endpoint.
(E) Primary tumor growth of FACS isolated $EMT6^{CaR}$ SM+ or $EMT6^{CaR}$ SM- tumor cells orthotopically implanted into Balb/c mice and treated with Veh or anti-PD-L1 with difference in the Gompertz model parameter β (specific growth rate increase) from growth kinetics analysis of primary tumor growth curves (top left inset of each graph).
(F) FC comparison of SM+ and SM- tumor responses to anti-PD-L1 antibody treatment (normalized to respective vehicle treated control and statistical analysis comparing treated SM+ and SM- groups) based on primary tumor volume.
(G) Overview schematic of proposed model.
*Parental (P); Cabozantinib-resistant (CaR); Fluorescent-activated cell sorting (FACS); Senescence-marker (SM); Ax (100mg/kg/day); anti-PD-L1 Ab (250ug/mouse/3 days); 5-Dodecanoylaminofluorescein Di-β-D-Galactopyranoside (C_{12}FDG); Vehicle treated control (Veh); See Appendix 3 for details of reduced Gompertz and mixed-effects modeling to evaluate tumor growth kinetics. Standard Deviation (SD); Primary tumor burden was assessed by caliper measurement. Quantitative data shown as mean ± SD. * $p< 0.05$; ** $p<0.01$.*

References

1. Upadhaya, S., Neftelinov, S.T., Hodge, J., and Campbell, J. (2022). Challenges and opportunities in the PD1/PDL1 inhibitor clinical trial landscape. Nat Rev Drug Discov. 10.1038/d41573-022-00030-4.
2. Vafaei, S., Zekiy, A.O., Khanamir, R.A., Zaman, B.A., Ghayourvahdat, A., Azimizonuzi, H., and Zamani, M. (2022). Combination therapy with immune checkpoint inhibitors (ICIs); a new frontier. Cancer Cell Int *22*, 2. 10.1186/s12935-021-02407-8.
3. Varayathu, H., Sarathy, V., Thomas, B.E., Mufti, S.S., and Naik, R. (2021). Combination Strategies to Augment Immune Check Point Inhibitors Efficacy - Implications for Translational Research. Front Oncol *11*, 559161. 10.3389/fonc.2021.559161.
4. Kohli, J., Wang, B., Brandenburg, S.M., Basisty, N., Evangelou, K., Varela-Eirin, M., Campisi, J., Schilling, B., Gorgoulis, V., and Demaria, M. (2021). Algorithmic assessment of cellular senescence in experimental and clinical specimens. Nat Protoc *16*, 2471-2498. 10.1038/s41596-021-00505-5.
5. Gonzalez-Gualda, E., Baker, A.G., Fruk, L., and Munoz-Espin, D. (2021). A guide to assessing cellular senescence in vitro and in vivo. FEBS J *288*, 56-80. 10.1111/febs.15570.
6. Davan-Wetton, C.S.A., Pessolano, E., Perretti, M., and Montero-Melendez, T. (2021). Senescence under appraisal: hopes and challenges revisited. Cell Mol Life Sci *78*, 3333-3354. 10.1007/s00018-020-03746-x.
7. Mastri, M., Tracz, A., Lee, C.R., Dolan, M., Attwood, K., Christensen, J.G., Liu, S., and Ebos, J.M.L. (2018). A Transient Pseudosenescent Secretome Promotes Tumor Growth after Antiangiogenic Therapy Withdrawal. Cell Rep *25*, 3706-3720 e3708. 10.1016/j.celrep.2018.12.017.
8. Mastri, M., and Ebos, J.M.L. (2019). Tumor growth fueled by spurious senescence phenotypes. Mol Cell Oncol *6*, 1575707. 10.1080/23723556.2019.1575707.
9. Sharpless, N.E., and Sherr, C.J. (2015). Forging a signature of in vivo senescence. Nat Rev Cancer *15*, 397-408. 10.1038/nrc3960.
10. Ewald, J.A., Desotelle, J.A., Wilding, G., and Jarrard, D.F. (2010). Therapy-induced senescence in cancer. J Natl Cancer Inst *102*, 1536-1546. 10.1093/jnci/djq364.
11. Coppe, J.P., Desprez, P.Y., Krtolica, A., and Campisi, J. (2010). The senescence-associated secretory phenotype: the dark side of tumor suppression. Annual review of pathology *5*, 99-118. 10.1146/annurev-pathol-121808-102144.
12. Ruscetti, M., Morris, J.P.t., Mezzadra, R., Russell, J., Leibold, J., Romesser, P.B., Simon, J., Kulick, A., Ho, Y.J., Fennell, M., et al. (2020). Senescence-Induced Vascular Remodeling Creates Therapeutic Vulnerabilities in Pancreas Cancer. Cell *181*, 424-441 e421. 10.1016/j.cell.2020.03.008.
13. Ruscetti, M., Leibold, J., Bott, M.J., Fennell, M., Kulick, A., Salgado, N.R., Chen, C.C., Ho, Y.J., Sanchez-Rivera, F.J., Feucht, J., et al. (2018). NK cell-mediated cytotoxicity contributes to tumor control by a cytostatic drug combination. Science *362*, 1416-1422. 10.1126/science.aas9090.
14. Tonnessen-Murray, C.A., Frey, W.D., Rao, S.G., Shahbandi, A., Ungerleider, N.A., Olayiwola, J.O., Murray, L.B., Vinson, B.T., Chrisey, D.B., Lord, C.J., and Jackson, J.G. (2019). Chemotherapy-induced senescent cancer cells engulf other cells to enhance their survival. J Cell Biol *218*, 3827-3844. 10.1083/jcb.201904051.
15. Duy, C., Li, M., Teater, M., Meydan, C., Garrett-Bakelman, F.E., Lee, T.C., Chin, C.R., Durmaz, C., Kawabata, K.C., Dhimolea, E., et al. (2021). Chemotherapy Induces Senescence-Like

Resilient Cells Capable of Initiating AML Recurrence. Cancer Discov *11*, 1542-1561. 10.1158/2159-8290.CD-20-1375.

16. Choi, Y.W., Kim, Y.H., Oh, S.Y., Suh, K.W., Kim, Y.S., Lee, G.Y., Yoon, J.E., Park, S.S., Lee, Y.K., Park, Y.J., et al. (2021). Senescent Tumor Cells Build a Cytokine Shield in Colorectal Cancer. Adv Sci (Weinh) *8*, 2002497. 10.1002/advs.202002497.
17. Iannello, A., Thompson, T.W., Ardolino, M., Lowe, S.W., and Raulet, D.H. (2013). p53-dependent chemokine production by senescent tumor cells supports NKG2D-dependent tumor elimination by natural killer cells. J Exp Med *210*, 2057-2069. 10.1084/jem.20130783.
18. Ovadya, Y., Landsberger, T., Leins, H., Vadai, E., Gal, H., Biran, A., Yosef, R., Sagiv, A., Agrawal, A., Shapira, A., et al. (2018). Impaired immune surveillance accelerates accumulation of senescent cells and aging. Nat Commun *9*, 5435. 10.1038/s41467-018-07825-3.
19. Cerboni, C., Fionda, C., Soriani, A., Zingoni, A., Doria, M., Cippitelli, M., and Santoni, A. (2014). The DNA Damage Response: A Common Pathway in the Regulation of NKG2D and DNAM-1 Ligand Expression in Normal, Infected, and Cancer Cells. Front Immunol *4*, 508. 10.3389/fimmu.2013.00508.
20. Krizhanovsky, V., Yon, M., Dickins, R.A., Hearn, S., Simon, J., Miething, C., Yee, H., Zender, L., and Lowe, S.W. (2008). Senescence of activated stellate cells limits liver fibrosis. Cell *134*, 657-667. 10.1016/j.cell.2008.06.049.
21. Egashira, M., Hirota, Y., Shimizu-Hirota, R., Saito-Fujita, T., Haraguchi, H., Matsumoto, L., Matsuo, M., Hiraoka, T., Tanaka, T., Akaeda, S., et al. (2017). F4/80+ Macrophages Contribute to Clearance of Senescent Cells in the Mouse Postpartum Uterus. Endocrinology *158*, 2344-2353. 10.1210/en.2016-1886.
22. Irvine, K.M., Skoien, R., Bokil, N.J., Melino, M., Thomas, G.P., Loo, D., Gabrielli, B., Hill, M.M., Sweet, M.J., Clouston, A.D., and Powell, E.E. (2014). Senescent human hepatocytes express a unique secretory phenotype and promote macrophage migration. World J Gastroenterol *20*, 17851-17862. 10.3748/wjg.v20.i47.17851.
23. Xue, W., Zender, L., Miething, C., Dickins, R.A., Hernando, E., Krizhanovsky, V., Cordon-Cardo, C., and Lowe, S.W. (2007). Senescence and tumour clearance is triggered by p53 restoration in murine liver carcinomas. Nature *445*, 656-660. 10.1038/nature05529.
24. Pereira, B.I., Devine, O.P., Vukmanovic-Stejic, M., Chambers, E.S., Subramanian, P., Patel, N., Virasami, A., Sebire, N.J., Kinsler, V., Valdovinos, A., et al. (2019). Senescent cells evade immune clearance via HLA-E-mediated NK and CD8(+) T cell inhibition. Nat Commun *10*, 2387. 10.1038/s41467-019-10335-5.
25. Ruhland, M.K., Loza, A.J., Capietto, A.H., Luo, X., Knolhoff, B.L., Flanagan, K.C., Belt, B.A., Alspach, E., Leahy, K., Luo, J., et al. (2016). Stromal senescence establishes an immunosuppressive microenvironment that drives tumorigenesis. Nat Commun *7*, 11762. 10.1038/ncomms11762.
26. Garcia-Diaz, A., Shin, D.S., Moreno, B.H., Saco, J., Escuin-Ordinas, H., Rodriguez, G.A., Zaretsky, J.M., Sun, L., Hugo, W., Wang, X., et al. (2017). Interferon Receptor Signaling Pathways Regulating PD-L1 and PD-L2 Expression. Cell reports *19*, 1189-1201. 10.1016/j.celrep.2017.04.031.
27. Yu, Q., Katlinskaya, Y.V., Carbone, C.J., Zhao, B., Katlinski, K.V., Zheng, H., Guha, M., Li, N., Chen, Q., Yang, T., et al. (2015). DNA-damage-induced type I interferon promotes senescence and inhibits stem cell function. Cell Rep *11*, 785-797. 10.1016/j.celrep.2015.03.069.
28. Frisch, S.M., and MacFawn, I.P. (2020). Type I interferons and related pathways in cell senescence. Aging Cell *19*, e13234. 10.1111/acel.13234.
29. Takahashi, A., Loo, T.M., Okada, R., Kamachi, F., Watanabe, Y., Wakita, M., Watanabe, S., Kawamoto, S., Miyata, K., Barber, G.N., et al. (2018). Downregulation of cytoplasmic DNases is implicated in cytoplasmic DNA accumulation and SASP in senescent cells. Nat Commun *9*, 1249. 10.1038/s41467-018-03555-8.

30. Dunphy, G., Flannery, S.M., Almine, J.F., Connolly, D.J., Paulus, C., Jonsson, K.L., Jakobsen, M.R., Nevels, M.M., Bowie, A.G., and Unterholzner, L. (2018). Non-canonical Activation of the DNA Sensing Adaptor STING by ATM and IFI16 Mediates NF-kappaB Signaling after Nuclear DNA Damage. Mol Cell *71*, 745-760 e745. 10.1016/j.molcel.2018.07.034.
31. Yang, H., Wang, H., Ren, J., Chen, Q., and Chen, Z.J. (2017). cGAS is essential for cellular senescence. Proc Natl Acad Sci U S A *114*, E4612-E4620. 10.1073/pnas.1705499114.
32. Falahat, R., Perez-Villarroel, P., Mailloux, A.W., Zhu, G., Pilon-Thomas, S., Barber, G.N., and Mule, J.J. (2019). STING Signaling in Melanoma Cells Shapes Antigenicity and Can Promote Antitumor T-cell Activity. Cancer immunology research *7*, 1837-1848. 10.1158/2326-6066.CIR-19-0229.
33. Brenner, E., Schorg, B.F., Ahmetlic, F., Wieder, T., Hilke, F.J., Simon, N., Schroeder, C., Demidov, G., Riedel, T., Fehrenbacher, B., et al. (2020). Cancer immune control needs senescence induction by interferon-dependent cell cycle regulator pathways in tumours. Nat Commun *11*, 1335. 10.1038/s41467-020-14987-6.
34. Abe, T., and Barber, G.N. (2014). Cytosolic-DNA-mediated, STING-dependent proinflammatory gene induction necessitates canonical NF-kappaB activation through TBK1. J Virol *88*, 5328-5341. 10.1128/JVI.00037-14.
35. Woo, S.R., Fuertes, M.B., Corrales, L., Spranger, S., Furdyna, M.J., Leung, M.Y., Duggan, R., Wang, Y., Barber, G.N., Fitzgerald, K.A., et al. (2014). STING-dependent cytosolic DNA sensing mediates innate immune recognition of immunogenic tumors. Immunity *41*, 830-842. 10.1016/j.immuni.2014.10.017.
36. Ishikawa, H., and Barber, G.N. (2008). STING is an endoplasmic reticulum adaptor that facilitates innate immune signalling. Nature *455*, 674-678. 10.1038/nature07317.
37. Georgilis, A., and Gil, J. (2016). Controlling secretion to limit chemoresistance. Genes Dev *30*, 1791-1792. 10.1101/gad.288571.116.
38. Velarde, M.C., and Demaria, M. (2016). Targeting Senescent Cells: Possible Implications for Delaying Skin Aging: A Mini-Review. Gerontology *62*, 513-518. 10.1159/000444877.
39. Tchkonia, T., Zhu, Y., van Deursen, J., Campisi, J., and Kirkland, J.L. (2013). Cellular senescence and the senescent secretory phenotype: therapeutic opportunities. J Clin Invest *123*, 966-972. 10.1172/JCI64098.
40. de Keizer, P.L. (2017). The Fountain of Youth by Targeting Senescent Cells? Trends Mol Med *23*, 6-17. 10.1016/j.molmed.2016.11.006.
41. Juers, D.H., Matthews, B.W., and Huber, R.E. (2012). LacZ beta-galactosidase: structure and function of an enzyme of historical and molecular biological importance. Protein Sci *21*, 1792-1807. 10.1002/pro.2165.
42. Debacq-Chainiaux, F., Erusalimsky, J.D., Campisi, J., and Toussaint, O. (2009). Protocols to detect senescence-associated beta-galactosidase (SA-betagal) activity, a biomarker of senescent cells in culture and in vivo. Nat Protoc *4*, 1798-1806. 10.1038/nprot.2009.191.
43. Morelli, M.B., Amantini, C., Santoni, M., Soriani, A., Nabissi, M., Cardinali, C., Santoni, A., and Santoni, G. (2015). Axitinib induces DNA damage response leading to senescence, mitotic catastrophe, and increased NK cell recognition in human renal carcinoma cells. Oncotarget *6*, 36245-36259. 10.18632/oncotarget.5768.
44. Coppe, J.P., Patil, C.K., Rodier, F., Sun, Y., Munoz, D.P., Goldstein, J., Nelson, P.S., Desprez, P.Y., and Campisi, J. (2008). Senescence-associated secretory phenotypes reveal cell-nonautonomous functions of oncogenic RAS and the p53 tumor suppressor. PLoS Biol *6*, 2853-2868. 10.1371/journal.pbio.0060301.
45. Rodier, F., Coppe, J.P., Patil, C.K., Hoeijmakers, W.A., Munoz, D.P., Raza, S.R., Freund, A., Campeau, E., Davalos, A.R., and Campisi, J. (2009). Persistent DNA damage signalling triggers senescence-associated inflammatory cytokine secretion. Nat Cell Biol *11*, 973-979. 10.1038/ncb1909.

46. Bent, E.H., Gilbert, L.A., and Hemann, M.T. (2016). A senescence secretory switch mediated by PI3K/AKT/mTOR activation controls chemoprotective endothelial secretory responses. Genes Dev *30*, 1811-1821. 10.1101/gad.284851.116.
47. Kuilman, T., Michaloglou, C., Vredeveld, L.C., Douma, S., van Doorn, R., Desmet, C.J., Aarden, L.A., Mooi, W.J., and Peeper, D.S. (2008). Oncogene-induced senescence relayed by an interleukin-dependent inflammatory network. Cell *133*, 1019-1031. 10.1016/j.cell.2008.03.039.
48. Obenauf, A.C., Zou, Y., Ji, A.L., Vanharanta, S., Shu, W., Shi, H., Kong, X., Bosenberg, M.C., Wiesner, T., Rosen, N., et al. (2015). Therapy-induced tumour secretomes promote resistance and tumour progression. Nature *520*, 368-372. 10.1038/nature14336.
49. Pribluda, A., Elyada, E., Wiener, Z., Hamza, H., Goldstein, R.E., Biton, M., Burstain, I., Morgenstern, Y., Brachya, G., Billauer, H., et al. (2013). A senescence-inflammatory switch from cancer-inhibitory to cancer-promoting mechanism. Cancer cell *24*, 242-256. 10.1016/j.ccr.2013.06.005.
50. Kuilman, T., and Peeper, D.S. (2009). Senescence-messaging secretome: SMS-ing cellular stress. Nat Rev Cancer *9*, 81-94. 10.1038/nrc2560.
51. Acosta, J.C., O'Loghlen, A., Banito, A., Guijarro, M.V., Augert, A., Raguz, S., Fumagalli, M., Da Costa, M., Brown, C., Popov, N., et al. (2008). Chemokine signaling via the CXCR2 receptor reinforces senescence. Cell *133*, 1006-1018. 10.1016/j.cell.2008.03.038.
52. Rusinova, I., Forster, S., Yu, S., Kannan, A., Masse, M., Cumming, H., Chapman, R., and Hertzog, P.J. (2013). Interferome v2.0: an updated database of annotated interferon-regulated genes. Nucleic Acids Res *41*, D1040-1046. 10.1093/nar/gks1215.
53. Grullich, C. (2018). Cabozantinib: Multi-kinase Inhibitor of MET, AXL, RET, and VEGFR2. Recent Results Cancer Res *211*, 67-75. 10.1007/978-3-319-91442-8_5.
54. Wood, C.G., Ferguson, J.E., 3rd, Parker, J.S., Moore, D.T., Whisenant, J.G., Maygarden, S.J., Wallen, E.M., Kim, W.Y., Milowsky, M.I., Beckermann, K.E., et al. (2020). Neoadjuvant pazopanib and molecular analysis of tissue response in renal cell carcinoma. JCI Insight *5*. 10.1172/jci.insight.132852.
55. Braga, S., Cardoso, J., Andre, S., Brito, M., Sanchez, P., Orvalho, L., Salgado, L., Dias, S., Pereira-Leal, J.B., and Passos-Coelho, J.L. (2017). Does Hypoxic Response Mediate Primary Resistance to Sunitinib in Untreated Locally Advanced Breast Cancer? Curr Cancer Drug Targets *17*, 62-73. 10.2174/1568009616666161025114914.
56. Diaz-Montero, C.M., Mao, F.J., Barnard, J., Parker, Y., Zamanian-Daryoush, M., Pink, J.J., Finke, J.H., Rini, B.I., and Lindner, D.J. (2016). MEK inhibition abrogates sunitinib resistance in a renal cell carcinoma patient-derived xenograft model. Br J Cancer *115*, 920-928. 10.1038/bjc.2016.263.
57. Pan, B.S., Perera, S.A., Piesvaux, J.A., Presland, J.P., Schroeder, G.K., Cumming, J.N., Trotter, B.W., Altman, M.D., Buevich, A.V., Cash, B., et al. (2020). An orally available non-nucleotide STING agonist with antitumor activity. Science *369*. 10.1126/science.aba6098.
58. Prantner, D., Perkins, D.J., Lai, W., Williams, M.S., Sharma, S., Fitzgerald, K.A., and Vogel, S.N. (2012). 5,6-Dimethylxanthenone-4-acetic acid (DMXAA) activates stimulator of interferon gene (STING)-dependent innate immune pathways and is regulated by mitochondrial membrane potential. J Biol Chem *287*, 39776-39788. 10.1074/jbc.M112.382986.
59. Conlon, J., Burdette, D.L., Sharma, S., Bhat, N., Thompson, M., Jiang, Z., Rathinam, V.A., Monks, B., Jin, T., Xiao, T.S., et al. (2013). Mouse, but not human STING, binds and signals in response to the vascular disrupting agent 5,6-dimethylxanthenone-4-acetic acid. J Immunol *190*, 5216-5225. 10.4049/jimmunol.1300097.
60. Braumuller, H., Wieder, T., Brenner, E., Assmann, S., Hahn, M., Alkhaled, M., Schilbach, K., Essmann, F., Kneilling, M., Griessinger, C., et al. (2013). T-helper-1-cell cytokines drive cancer into senescence. Nature *494*, 361-365. 10.1038/nature11824.

61. De Cecco, M., Ito, T., Petrashen, A.P., Elias, A.E., Skvir, N.J., Criscione, S.W., Caligiana, A., Brocculi, G., Adney, E.M., Boeke, J.D., et al. (2019). L1 drives IFN in senescent cells and promotes age-associated inflammation. Nature *566*, 73-78. 10.1038/s41586-018-0784-9.
62. Trinchieri, G. (2010). Type I interferon: friend or foe? J Exp Med *207*, 2053-2063. 10.1084/jem.20101664.
63. Fenton, S.E., Saleiro, D., and Platanias, L.C. (2021). Type I and II Interferons in the Anti-Tumor Immune Response. Cancers (Basel) *13*. 10.3390/cancers13051037.
64. Marin, I., Boix, O., Garcia-Garijo, A., Sirois, I., Caballe, A., Zarzuela, E., Ruano, I., Attolini, C.S., Prats, N., Lopez-Dominguez, J.A., et al. (2023). Cellular Senescence Is Immunogenic and Promotes Antitumor Immunity. Cancer discovery *13*, 410-431. 10.1158/2159-8290.CD-22-0523.
65. Vaghi, C., Rodallec, A., Fanciullino, R., Ciccolini, J., Mochel, J.P., Mastri, M., Poignard, C., Ebos, J.M.L., and Benzekry, S. (2020). Population modeling of tumor growth curves and the reduced Gompertz model improve prediction of the age of experimental tumors. PLoS Comput Biol *16*, e1007178. 10.1371/journal.pcbi.1007178.
66. Quah, B.J., and Parish, C.R. (2010). The use of carboxyfluorescein diacetate succinimidyl ester (CFSE) to monitor lymphocyte proliferation. J Vis Exp. 10.3791/2259.
67. Medema, J.P., de Jong, J., Peltenburg, L.T., Verdegaal, E.M., Gorter, A., Bres, S.A., Franken, K.L., Hahne, M., Albar, J.P., Melief, C.J., and Offringa, R. (2001). Blockade of the granzyme B/perforin pathway through overexpression of the serine protease inhibitor PI-9/SPI-6 constitutes a mechanism for immune escape by tumors. Proc Natl Acad Sci U S A *98*, 11515-11520. 10.1073/pnas.201398198.
68. Mosely, S.I., Prime, J.E., Sainson, R.C., Koopmann, J.O., Wang, D.Y., Greenawalt, D.M., Ahdesmaki, M.J., Leyland, R., Mullins, S., Pacelli, L., et al. (2017). Rational Selection of Syngeneic Preclinical Tumor Models for Immunotherapeutic Drug Discovery. Cancer immunology research *5*, 29-41. 10.1158/2326-6066.CIR-16-0114.
69. Mall, C., Sckisel, G.D., Proia, D.A., Mirsoian, A., Grossenbacher, S.K., Pai, C.S., Chen, M., Monjazeb, A.M., Kelly, K., Blazar, B.R., and Murphy, W.J. (2016). Repeated PD-1/PD-L1 monoclonal antibody administration induces fatal xenogeneic hypersensitivity reactions in a murine model of breast cancer. Oncoimmunology *5*, e1075114. 10.1080/2162402X.2015.1075114.
70. Monjazeb, A.M., Wang, Z., Vick, L.V., Dunai, C., Minnar, C., Khuat, L.T., and Murphy, W.J. (2021). Mouse Preclinical Cancer Immunotherapy Modeling Involving Anti-PD-1 Therapies Reveals the Need to Use Mouse Reagents to Mirror Clinical Paradigms. Cancers (Basel) *13*. 10.3390/cancers13040729.
71. Motzer, R.J., Penkov, K., Haanen, J., Rini, B., Albiges, L., Campbell, M.T., Venugopal, B., Kollmannsberger, C., Negrier, S., Uemura, M., et al. (2019). Avelumab plus Axitinib versus Sunitinib for Advanced Renal-Cell Carcinoma. N Engl J Med *380*, 1103-1115. 10.1056/NEJMoa1816047.
72. Rini, B.I., Plimack, E.R., Stus, V., Gafanov, R., Hawkins, R., Nosov, D., Pouliot, F., Alekseev, B., Soulieres, D., Melichar, B., et al. (2019). Pembrolizumab plus Axitinib versus Sunitinib for Advanced Renal-Cell Carcinoma. N Engl J Med *380*, 1116-1127. 10.1056/NEJMoa1816714.
73. Motzer, R.J., Robbins, P.B., Powles, T., Albiges, L., Haanen, J.B., Larkin, J., Mu, X.J., Ching, K.A., Uemura, M., Pal, S.K., et al. (2020). Avelumab plus axitinib versus sunitinib in advanced renal cell carcinoma: biomarker analysis of the phase 3 JAVELIN Renal 101 trial. Nat Med. 10.1038/s41591-020-1044-8.
74. Choueiri, T.K., Powles, T., Burotto, M., Escudier, B., Bourlon, M.T., Zurawski, B., Oyervides Juarez, V.M., Hsieh, J.J., Basso, U., Shah, A.Y., et al. (2021). Nivolumab plus Cabozantinib versus Sunitinib for Advanced Renal-Cell Carcinoma. N Engl J Med *384*, 829-841. 10.1056/NEJMoa2026982.

75. Heine, A., Held, S.A., Bringmann, A., Holderried, T.A., and Brossart, P. (2011). Immunomodulatory effects of anti-angiogenic drugs. Leukemia *25*, 899-905. 10.1038/leu.2011.24.
76. Stehle, F., Schulz, K., Fahldieck, C., Kalich, J., Lichtenfels, R., Riemann, D., and Seliger, B. (2013). Reduced immunosuppressive properties of axitinib in comparison with other tyrosine kinase inhibitors. J Biol Chem *288*, 16334-16347. 10.1074/jbc.M112.437962.
77. Prasanna, P.G., Citrin, D.E., Hildesheim, J., Ahmed, M.M., Venkatachalam, S., Riscuta, G., Xi, D., Zheng, G., Deursen, J.V., Goronzy, J., et al. (2021). Therapy-Induced Senescence: Opportunities to Improve Anticancer Therapy. J Natl Cancer Inst *113*, 1285-1298. 10.1093/jnci/djab064.
78. Wang, L., Lankhorst, L., and Bernards, R. (2022). Exploiting senescence for the treatment of cancer. Nat Rev Cancer *22*, 340-355. 10.1038/s41568-022-00450-9.
79. Zhang, L., Pitcher, L.E., Prahalad, V., Niedernhofer, L.J., and Robbins, P.D. (2023). Targeting cellular senescence with senotherapeutics: senolytics and senomorphics. FEBS J *290*, 1362-1383. 10.1111/febs.16350.
80. Wang, B., and Demaria, M. (2021). The Quest to Define and Target Cellular Senescence in Cancer. Cancer Res *81*, 6087-6089. 10.1158/0008-5472.CAN-21-2032.
81. Lee, S., and Schmitt, C.A. (2019). The dynamic nature of senescence in cancer. Nat Cell Biol *21*, 94-101. 10.1038/s41556-018-0249-2.
82. Chakradeo, S., Elmore, L.W., and Gewirtz, D.A. (2016). Is Senescence Reversible? Curr Drug Targets *17*, 460-466.
83. Romaniello, D., Gelfo, V., Pagano, F., Ferlizza, E., Sgarzi, M., Mazzeschi, M., Morselli, A., Miano, C., D'Uva, G., and Lauriola, M. (2022). Senescence-associated reprogramming induced by interleukin-1 impairs response to EGFR neutralization. Cell Mol Biol Lett *27*, 20. 10.1186/s11658-022-00319-7.
84. Salunkhe, S., Mishra, S.V., Nair, J., Shah, S., Gardi, N., Thorat, R., Sarkar, D., Rajendra, J., Kaur, E., and Dutt, S. (2021). Nuclear localization of p65 reverses therapy-induced senescence. J Cell Sci *134*. 10.1242/jcs.253203.
85. Bollard, J., Miguela, V., Ruiz de Galarreta, M., Venkatesh, A., Bian, C.B., Roberto, M.P., Tovar, V., Sia, D., Molina-Sanchez, P., Nguyen, C.B., et al. (2017). Palbociclib (PD-0332991), a selective CDK4/6 inhibitor, restricts tumour growth in preclinical models of hepatocellular carcinoma. Gut *66*, 1286-1296. 10.1136/gutjnl-2016-312268.
86. Maskey, R.S., Wang, F., Lehman, E., Wang, Y., Emmanuel, N., Zhong, W., Jin, G., Abraham, R.T., Arndt, K.T., Myers, J.S., and Mazurek, A. (2021). Sustained mTORC1 activity during palbociclib-induced growth arrest triggers senescence in ER+ breast cancer cells. Cell Cycle *20*, 65-80. 10.1080/15384101.2020.1859195.
87. Fleury, H., Malaquin, N., Tu, V., Gilbert, S., Martinez, A., Olivier, M.A., Sauriol, A., Communal, L., Leclerc-Desaulniers, K., Carmona, E., et al. (2019). Exploiting interconnected synthetic lethal interactions between PARP inhibition and cancer cell reversible senescence. Nat Commun *10*, 2556. 10.1038/s41467-019-10460-1.
88. Madorsky Rowdo, F.P., Baron, A., von Euw, E.M., and Mordoh, J. (2017). In vitro long-term treatment with MAPK inhibitors induces melanoma cells with resistance plasticity to inhibitors while retaining sensitivity to CD8 T cells. Oncol Rep *37*, 1367-1378. 10.3892/or.2017.5363.
89. Kurppa, K.J., Liu, Y., To, C., Zhang, T., Fan, M., Vajdi, A., Knelson, E.H., Xie, Y., Lim, K., Cejas, P., et al. (2020). Treatment-Induced Tumor Dormancy through YAP-Mediated Transcriptional Reprogramming of the Apoptotic Pathway. Cancer Cell *37*, 104-122 e112. 10.1016/j.ccell.2019.12.006.
90. Hu, Z., Yuan, J., Long, M., Jiang, J., Zhang, Y., Zhang, T., Xu, M., Fan, Y., Tanyi, J.L., Montone, K.T., et al. (2021). The Cancer Surfaceome Atlas integrates genomic, functional and drug response data to identify actionable targets. Nat Cancer *2*, 1406-1422. 10.1038/s43018-021-00282-w.

91. Saleh, T., Tyutyunyk-Massey, L., Murray, G.F., Alotaibi, M.R., Kawale, A.S., Elsayed, Z., Henderson, S.C., Yakovlev, V., Elmore, L.W., Toor, A., et al. (2019). Tumor cell escape from therapy-induced senescence. Biochem Pharmacol *162*, 202-212. 10.1016/j.bcp.2018.12.013.
92. Hao, X., Zhao, B., Zhou, W., Liu, H., Fukumoto, T., Gabrilovich, D., and Zhang, R. (2021). Sensitization of ovarian tumor to immune checkpoint blockade by boosting senescence-associated secretory phenotype. iScience *24*, 102016. 10.1016/j.isci.2020.102016.
93. Paffenholz, S.V., Salvagno, C., Ho, Y.J., Limjoco, M., Baslan, T., Tian, S., Kulick, A., de Stanchina, E., Wilkinson, J.E., Barriga, F.M., et al. (2022). Senescence induction dictates response to chemo- and immunotherapy in preclinical models of ovarian cancer. Proc Natl Acad Sci U S A *119*. 10.1073/pnas.2117754119.
94. Pantelidou, C., Sonzogni, O., De Oliveria Taveira, M., Mehta, A.K., Kothari, A., Wang, D., Visal, T., Li, M.K., Pinto, J., Castrillon, J.A., et al. (2019). PARP Inhibitor Efficacy Depends on CD8(+) T-cell Recruitment via Intratumoral STING Pathway Activation in BRCA-Deficient Models of Triple-Negative Breast Cancer. Cancer Discov *9*, 722-737. 10.1158/2159-8290.CD-18-1218.
95. Jing, W., McAllister, D., Vonderhaar, E.P., Palen, K., Riese, M.J., Gershan, J., Johnson, B.D., and Dwinell, M.B. (2019). STING agonist inflames the pancreatic cancer immune microenvironment and reduces tumor burden in mouse models. J Immunother Cancer *7*, 115. 10.1186/s40425-019-0573-5.
96. Sistigu, A., Yamazaki, T., Vacchelli, E., Chaba, K., Enot, D.P., Adam, J., Vitale, I., Goubar, A., Baracco, E.E., Remedios, C., et al. (2014). Cancer cell-autonomous contribution of type I interferon signaling to the efficacy of chemotherapy. Nat Med *20*, 1301-1309. 10.1038/nm.3708.
97. Adachi, Y., Kamiyama, H., Ichikawa, K., Fukushima, S., Ozawa, Y., Yamaguchi, S., Goda, S., Kimura, T., Kodama, K., Matsuki, M., et al. (2022). Inhibition of FGFR Reactivates IFNgamma Signaling in Tumor Cells to Enhance the Combined Antitumor Activity of Lenvatinib with Anti-PD-1 Antibodies. Cancer Res *82*, 292-306. 10.1158/0008-5472.CAN-20-2426.
98. Goel, S., DeCristo, M.J., Watt, A.C., BrinJones, H., Sceneay, J., Li, B.B., Khan, N., Ubellacker, J.M., Xie, S., Metzger-Filho, O., et al. (2017). CDK4/6 inhibition triggers anti-tumour immunity. Nature *548*, 471-475. 10.1038/nature23465.
99. Yang, H., Lee, W.S., Kong, S.J., Kim, C.G., Kim, J.H., Chang, S.K., Kim, S., Kim, G., Chon, H.J., and Kim, C. (2019). STING activation reprograms tumor vasculatures and synergizes with VEGFR2 blockade. J Clin Invest *129*, 4350-4364. 10.1172/JCI125413.
100. Dimri, G.P., Lee, X., Basile, G., Acosta, M., Scott, G., Roskelley, C., Medrano, E.E., Linskens, M., Rubelj, I., Pereira-Smith, O., and et al. (1995). A biomarker that identifies senescent human cells in culture and in aging skin in vivo. Proc Natl Acad Sci U S A *92*, 9363-9367. 10.1073/pnas.92.20.9363.
101. Kurz, D.J., Decary, S., Hong, Y., and Erusalimsky, J.D. (2000). Senescence-associated (beta)-galactosidase reflects an increase in lysosomal mass during replicative ageing of human endothelial cells. J Cell Sci *113 (Pt 20)*, 3613-3622. 10.1242/jcs.113.20.3613.
102. Lee, B.Y., Han, J.A., Im, J.S., Morrone, A., Johung, K., Goodwin, E.C., Kleijer, W.J., DiMaio, D., and Hwang, E.S. (2006). Senescence-associated beta-galactosidase is lysosomal beta-galactosidase. Aging Cell *5*, 187-195. 10.1111/j.1474-9726.2006.00199.x.
103. Ruzickova, E., Skoupa, N., Dolezel, P., Smith, D.A., and Mlejnek, P. (2019). The Lysosomal Sequestration of Tyrosine Kinase Inhibitors and Drug Resistance. Biomolecules *9*. 10.3390/biom9110675.
104. Gotink, K.J., Broxterman, H.J., Labots, M., de Haas, R.R., Dekker, H., Honeywell, R.J., Rudek, M.A., Beerepoot, L.V., Musters, R.J., Jansen, G., et al. (2011). Lysosomal sequestration of sunitinib: a novel mechanism of drug resistance. Clin Cancer Res *17*, 7337-7346. 10.1158/1078-0432.CCR-11-1667.
105. Fassl, A., Brain, C., Abu-Remaileh, M., Stukan, I., Butter, D., Stepien, P., Feit, A.S., Bergholz, J., Michowski, W., Otto, T., et al. (2020). Increased lysosomal biomass is responsible for the

resistance of triple-negative breast cancers to CDK4/6 inhibition. Sci Adv *6*, eabb2210. 10.1126/sciadv.abb2210.

106. Colombo, F., Trombetta, E., Cetrangolo, P., Maggioni, M., Razini, P., De Santis, F., Torrente, Y., Prati, D., Torresani, E., and Porretti, L. (2014). Giant Lysosomes as a Chemotherapy Resistance Mechanism in Hepatocellular Carcinoma Cells. PLoS One *9*, e114787. 10.1371/journal.pone.0114787.
107. Zhang, H., Zoued, A., Liu, X., Sit, B., and Waldor, M.K. (2020). Type I interferon remodels lysosome function and modifies intestinal epithelial defense. Proc Natl Acad Sci U S A *117*, 29862-29871. 10.1073/pnas.2010723117.
108. Unterholzner, L., and Dunphy, G. (2019). cGAS-independent STING activation in response to DNA damage. Mol Cell Oncol *6*, 1558682. 10.1080/23723556.2018.1558682.
109. Elgendy, M., Abdel-Aziz, A.K., Renne, S.L., Bornaghi, V., Procopio, G., Colecchia, M., Kanesvaran, R., Toh, C.K., Bossi, D., Pallavicini, I., et al. (2017). Dual modulation of MCL-1 and mTOR determines the response to sunitinib. J Clin Invest *127*, 153-168. 10.1172/JCI84386.
110. Jimenez-Valerio, G., Martinez-Lozano, M., Bassani, N., Vidal, A., Ochoa-de-Olza, M., Suarez, C., Garcia-Del-Muro, X., Carles, J., Vinals, F., Graupera, M., et al. (2016). Resistance to Antiangiogenic Therapies by Metabolic Symbiosis in Renal Cell Carcinoma PDX Models and Patients. Cell Rep *15*, 1134-1143. 10.1016/j.celrep.2016.04.015.
111. Zhang, L., Wei, X., Wang, Z., Liu, P., Hou, Y., Xu, Y., Su, H., Koci, M.D., Yin, H., and Zhang, C. (2023). NF-kappaB activation enhances STING signaling by altering microtubule-mediated STING trafficking. Cell Rep *42*, 112185. 10.1016/j.celrep.2023.112185.
112. Benci, J.L., Xu, B., Qiu, Y., Wu, T.J., Dada, H., Twyman-Saint Victor, C., Cucolo, L., Lee, D.S.M., Pauken, K.E., Huang, A.C., et al. (2016). Tumor Interferon Signaling Regulates a Multigenic Resistance Program to Immune Checkpoint Blockade. Cell *167*, 1540-1554 e1512. 10.1016/j.cell.2016.11.022.
113. Shi, Y., Dolan, M., Mastri, M., Hill, J.W., Dommer, A., Benzekry, S., Eng, K., and Ebos, J.M.L. (2021). Acquired resistance to PD-L1 inhibition is associated with an enhanced type I IFN-stimulated secretory program in tumor cells. bioRxiv, 2021.2007.2001.450417. 10.1101/2021.07.01.450417.
114. Jacquelot, N., Yamazaki, T., Roberti, M.P., Duong, C.P.M., Andrews, M.C., Verlingue, L., Ferrere, G., Becharef, S., Vetizou, M., Daillere, R., et al. (2019). Sustained Type I interferon signaling as a mechanism of resistance to PD-1 blockade. Cell Res *29*, 846-861. 10.1038/s41422-019-0224-x.
115. Dolan, M., Mastri, M., Tracz, A., Christensen, J.G., Chatta, G., and Ebos, J.M.L. (2019). Enhanced efficacy of sitravatinib in metastatic models of antiangiogenic therapy resistance. PLoS One *14*, e0220101. 10.1371/journal.pone.0220101.
116. Ebos, J.M., Mastri, M., Lee, C.R., Tracz, A., Hudson, J.M., Attwood, K., Cruz-Munoz, W.R., Jedeszko, C., Burns, P., and Kerbel, R.S. (2014). Neoadjuvant antiangiogenic therapy reveals contrasts in primary and metastatic tumor efficacy. EMBO Mol Med *6*, 1561-1576. 10.15252/emmm.201403989.
117. Ebos, J.M., Lee, C.R., Bogdanovic, E., Alami, J., Van Slyke, P., Francia, G., Xu, P., Mutsaers, A.J., Dumont, D.J., and Kerbel, R.S. (2008). Vascular endothelial growth factor-mediated decrease in plasma soluble vascular endothelial growth factor receptor-2 levels as a surrogate biomarker for tumor growth. Cancer Res *68*, 521-529. 10.1158/0008-5472.CAN-07-3217.
118. Tracz, A., Mastri, M., Lee, C.R., Pili, R., and Ebos, J.M. (2014). Modeling spontaneous metastatic renal cell carcinoma (mRCC) in mice following nephrectomy. J Vis Exp. 10.3791/51485.
119. Mundra, P.A., and Rajapakse, J.C. (2016). Gene and sample selection using T-score with sample selection. J Biomed Inform *59*, 31-41. 10.1016/j.jbi.2015.11.003.

Figure 1

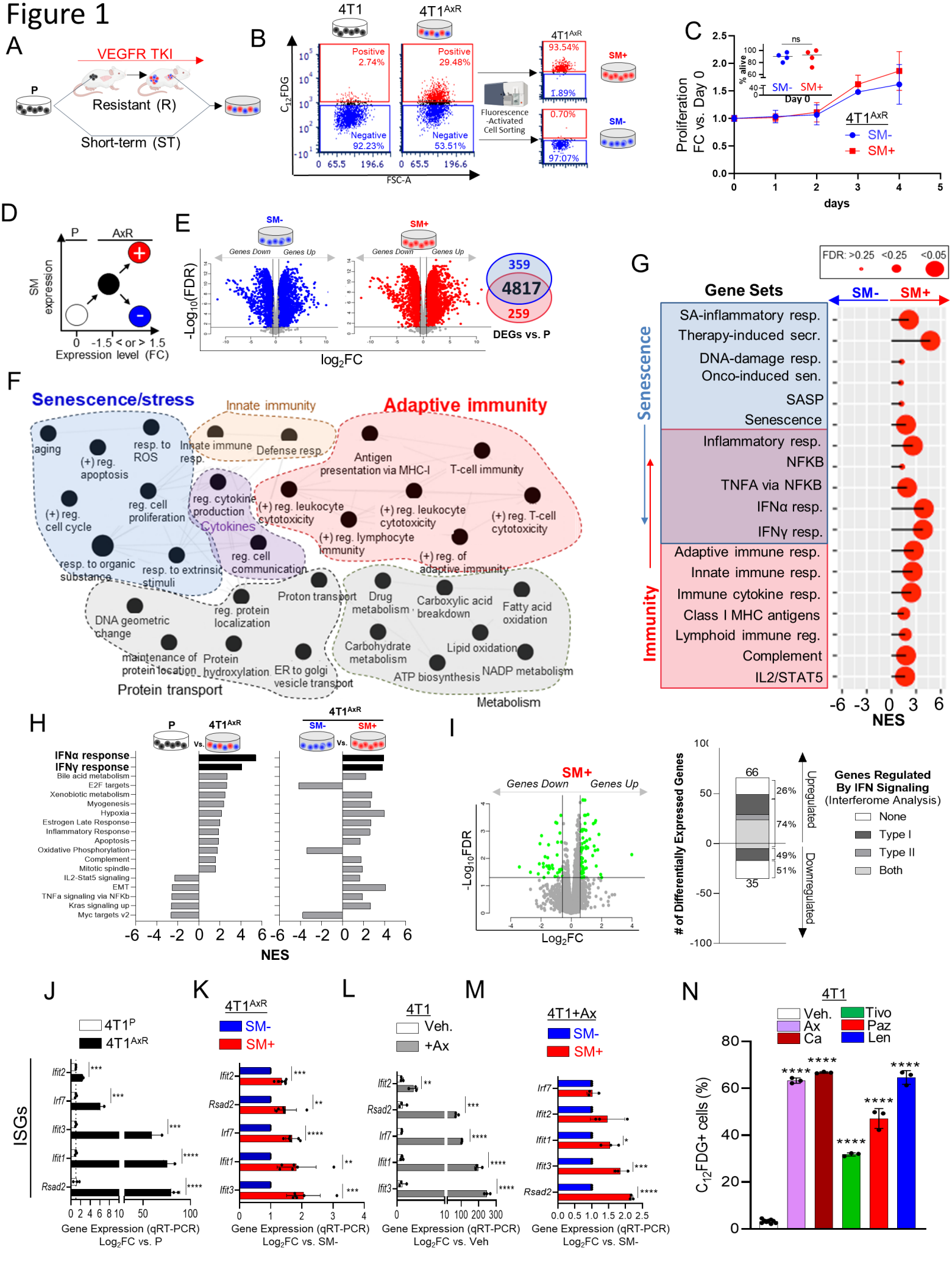
A
VEGFR TKI
P
Resistant (R)
Short-term (ST)
B
4T1
4T1AxR
Positive 2.74%
Positive 29.48%
Negative 92.23%
Negative 53.51%
C12FDG
FSC-A
Fluorescence -Activated Cell Sorting
93.54%
1.89%
0.70%
97.07%
SM+
SM-
C
Proliferation FC vs. Day 0
% alive
ns
Day 0
days
D
P
AxR
SM expression
Expression level (FC)
E
SM-
SM+
Genes Down
Genes Up
-Log10(FDR)
log2FC
359
4817
259
DEGs vs. P
F
Senescence/stress
Innate immunity
Adaptive immunity
aging
(+) reg. apoptosis
resp. to ROS
Innate immune resp.
Defense resp.
Antigen presentation via MHC-I
T-cell immunity
(+) reg. cell cycle
reg. cell proliferation
reg. cytokine production
Cytokines
(+) reg. leukocyte cytotoxicity
(+) reg. leukocyte cytotoxicity
(+) reg. T-cell cytotoxicity
(+) reg. lymphocyte immunity
(+) reg. of adaptive immunity
resp. to organic substance
resp. to extrinsic stimuli
reg. cell communication
Proton transport
Drug metabolism
Carboxylic acid breakdown
Fatty acid oxidation
DNA geometric change
reg. protein localization
Carbohydrate metabolism
Lipid oxidation
maintenance of protein location
Protein hydroxylation
ER to golgi vesicle transport
ATP biosynthesis
NADP metabolism
Protein transport
Metabolism
G
FDR: >0.25 <0.25 <0.05
Gene Sets
SM-
SM+
Senescence
Immunity
SA-inflammatory resp.
Therapy-induced secr.
DNA-damage resp.
Onco-induced sen.
SASP
Senescence
Inflammatory resp.
NFKB
TNFA via NFKB
IFNα resp.
IFNγ resp.
Adaptive immune resp.
Innate immune resp.
Immune cytokine resp.
Class I MHC antigens
Lymphoid immune reg.
Complement
IL2/STAT5
NES
H
P
4T1AxR
Vs.
SM-
SM+
IFNα response
IFNγ response
Bile acid metabolism
E2F targets
Xenobiotic metabolism
Myogenesis
Hypoxia
Estrogen Late Response
Inflammatory Response
Apoptosis
Oxidative Phosphorylation
Complement
Mitotic spindle
IL2-Stat5 signaling
EMT
TNFa signaling via NFKb
Kras signaling up
Myc targets v2
NES
I
SM+
Genes Down
Genes Up
-Log10FDR
Log2FC
# of Differentially Expressed Genes
66
35
26%
74%
49%
51%
Upregulated
Downregulated
Genes Regulated By IFN Signaling
(Interferome Analysis)
None
Type I
Type II
Both
J
4T1P
4T1AxR
ISGs
Ifit2
Irf7
Ifit3
Ifit1
Rsad2
Gene Expression (qRT-PCR)
Log2FC vs. P
K
4T1AxR
SM-
SM+
Gene Expression (qRT-PCR)
Log2FC vs. SM-
L
4T1
Veh.
+Ax
Gene Expression (qRT-PCR)
Log2FC vs. Veh
M
4T1+Ax
SM-
SM+
Gene Expression (qRT-PCR)
Log2FC vs. SM-
N
4T1
Veh.
Ax
Ca
Tivo
Paz
Len
C12FDG+ cells (%)

Figure 2

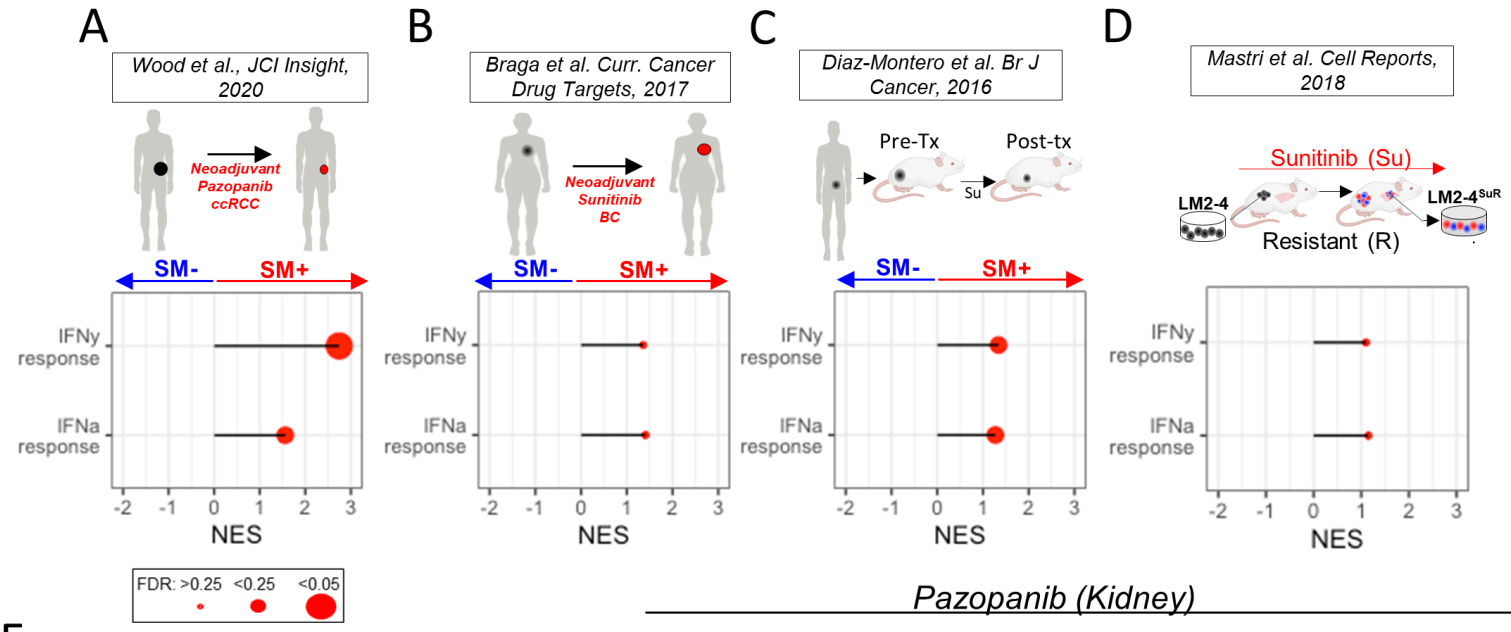
A
Wood et al., JCI Insight, 2020
Neoadjuvant Pazopanib ccRCC
B
Braga et al. Curr. Cancer Drug Targets, 2017
Neoadjuvant Sunitinib BC
C
Diaz-Montero et al. Br J Cancer, 2016
Pre-Tx
Post-tx
Su
D
Mastri et al. Cell Reports, 2018
Sunitinib (Su)
LM2-4
LM2-4SuR
Resistant (R)
SM-
SM+
IFNy response
IFNa response
NES
FDR: >0.25 <0.25 <0.05

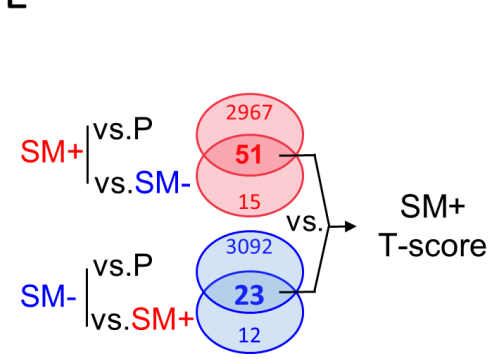
E
SM+
vs.P
vs.SM-
2967
51
15
SM-
vs.P
vs.SM+
3092
23
12
vs.
SM+ T-score

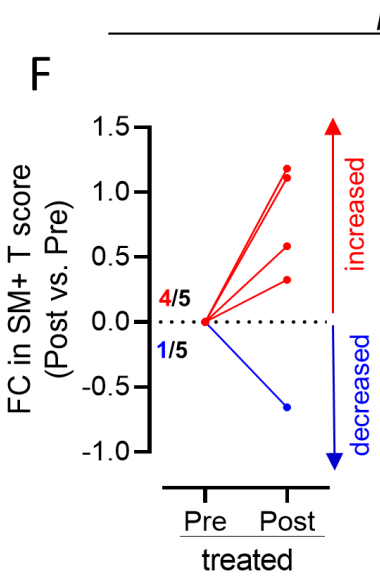
Pazopanib (Kidney)
F
FC in SM+ T score (Post vs. Pre)
4/5
1/5
increased
decreased
Pre
Post
treated

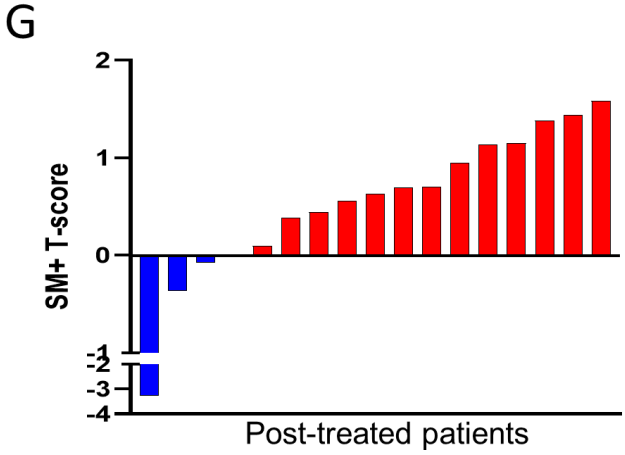
G
SM+ T-score
Post-treated patients

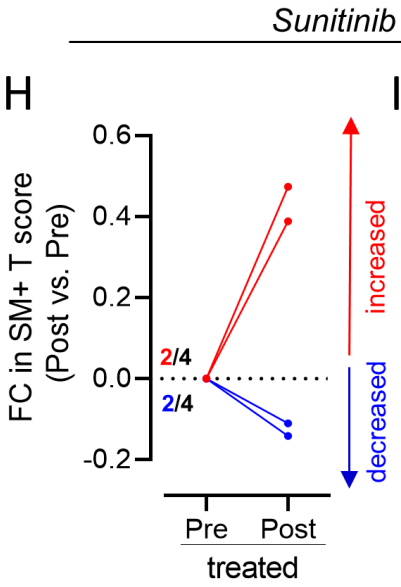
Sunitinib (Breast)
H
FC in SM+ T score (Post vs. Pre)
2/4
2/4
increased
decreased
Pre
Post
treated

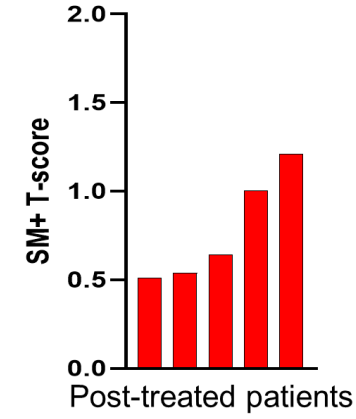
I
SM+ T-score
Post-treated patients

Figure 3

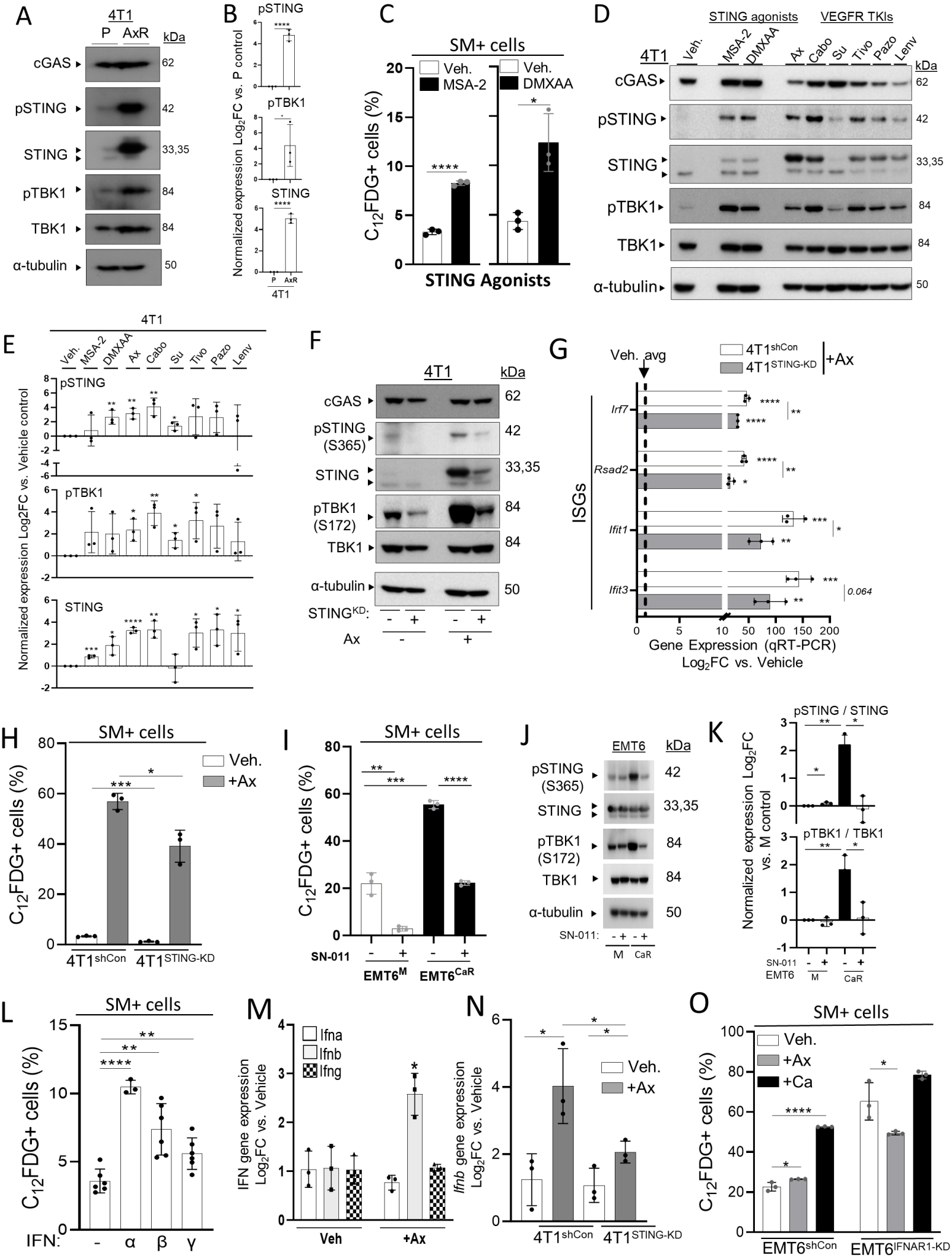
A
4T1
P
AxR
kDa
cGAS
62
pSTING
42
STING
33,35
pTBK1
84
TBK1
84
α-tubulin
50
B
pSTING
pTBK1
STING
Normalized expression Log2FC vs. P control
P
AxR
4T1
C
SM+ cells
Veh.
MSA-2
Veh.
DMXAA
C12FDG+ cells (%)
STING Agonists
D
STING agonists
VEGFR TKIs
4T1
Veh.
MSA-2
DMXAA
Ax
Cabo
Su
Tivo
Pazo
Lenv
kDa
cGAS
62
pSTING
42
STING
33,35
pTBK1
84
TBK1
84
α-tubulin
50
E
4T1
Veh.
MSA-2
DMXAA
Ax
Cabo
Su
Tivo
Pazo
Lenv
pSTING
pTBK1
STING
Normalized expression Log2FC vs. Vehicle control
F
4T1
kDa
cGAS
62
pSTING (S365)
42
STING
33,35
pTBK1 (S172)
84
TBK1
84
α-tubulin
50
STINGKD:
Ax
G
Veh. avg
4T1shCon
4T1STING-KD
+Ax
Irf7
Rsad2
Ifit1
Ifit3
0.064
ISGs
Gene Expression (qRT-PCR)
Log2FC vs. Vehicle
H
SM+ cells
Veh.
+Ax
C12FDG+ cells (%)
4T1shCon
4T1STING-KD
I
SM+ cells
C12FDG+ cells (%)
SN-011
EMT6M
EMT6CaR
J
EMT6
kDa
pSTING (S365)
42
STING
33,35
pTBK1 (S172)
84
TBK1
84
α-tubulin
50
SN-011:
M
CaR
K
pSTING / STING
pTBK1 / TBK1
Normalized expression Log2FC vs. M control
SN-011
EMT6
M
CaR
L
SM+ cells
C12FDG+ cells (%)
IFN:
-
α
β
γ
M
Ifna
Ifnb
Ifng
IFN gene expression Log2FC vs. Vehicle
Veh
+Ax
N
Veh.
+Ax
Ifnb gene expression Log2FC vs. Vehicle
4T1shCon
4T1STING-KD
O
SM+ cells
Veh.
+Ax
+Ca
C12FDG+ cells (%)
EMT6shCon
EMT6IFNAR1-KD

Figure 4

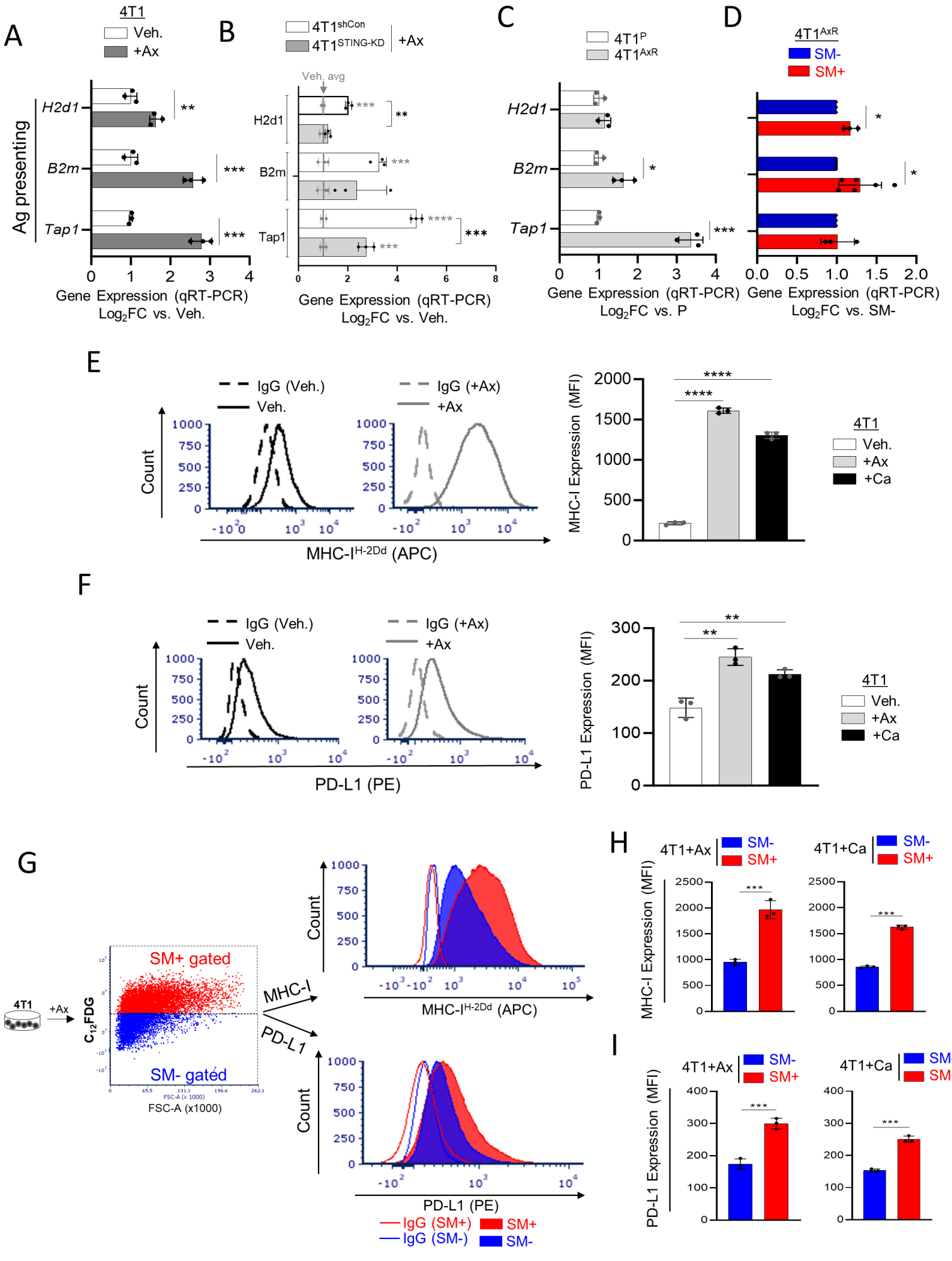
A
4T1
Veh.
+Ax
Ag presenting
H2d1
B2m
Tap1
Gene Expression (qRT-PCR)
Log2FC vs. Veh.
B
4T1shCon
4T1STING-KD
+Ax
Veh. avg
C
4T1P
4T1AxR
Log2FC vs. P
D
4T1AxR
SM-
SM+
Log2FC vs. SM-
E
IgG (Veh.)
Veh.
IgG (+Ax)
+Ax
Count
MHC-IH-2Dd (APC)
MHC-I Expression (MFI)
4T1
Veh.
+Ax
+Ca
F
PD-L1 (PE)
PD-L1 Expression (MFI)
G
4T1
+Ax
C12FDG
SM+ gated
SM- gated
FSC-A (x1000)
MHC-I
PD-L1
IgG (SM+)
IgG (SM-)
SM+
SM-
H
4T1+Ax
4T1+Ca
I

Figure 5

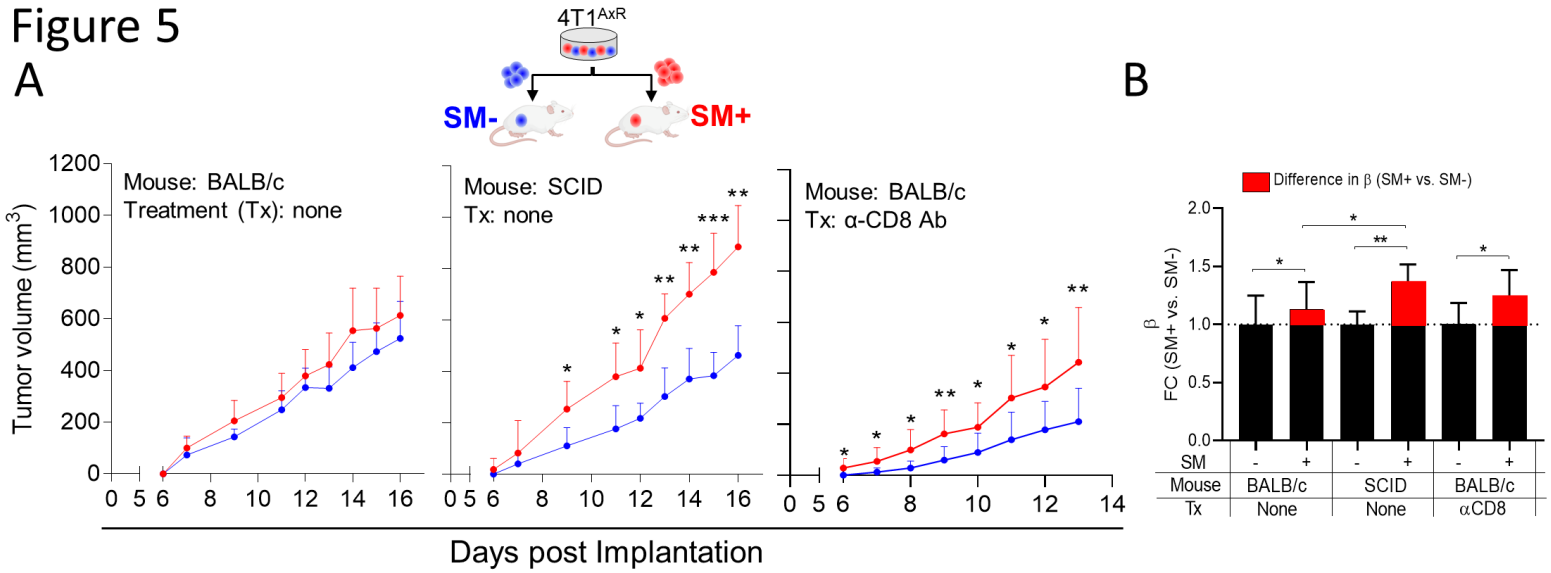
A
4T1AxR
SM-
SM+
Mouse: BALB/c
Treatment (Tx): none
Mouse: SCID
Tx: none
Mouse: BALB/c
Tx: α-CD8 Ab
Tumor volume (mm3)
Days post Implantation
B
Difference in β (SM+ vs. SM-)
β FC (SM+ vs. SM-)
SM
Mouse
Tx
BALB/c
SCID
BALB/c
None
None
αCD8

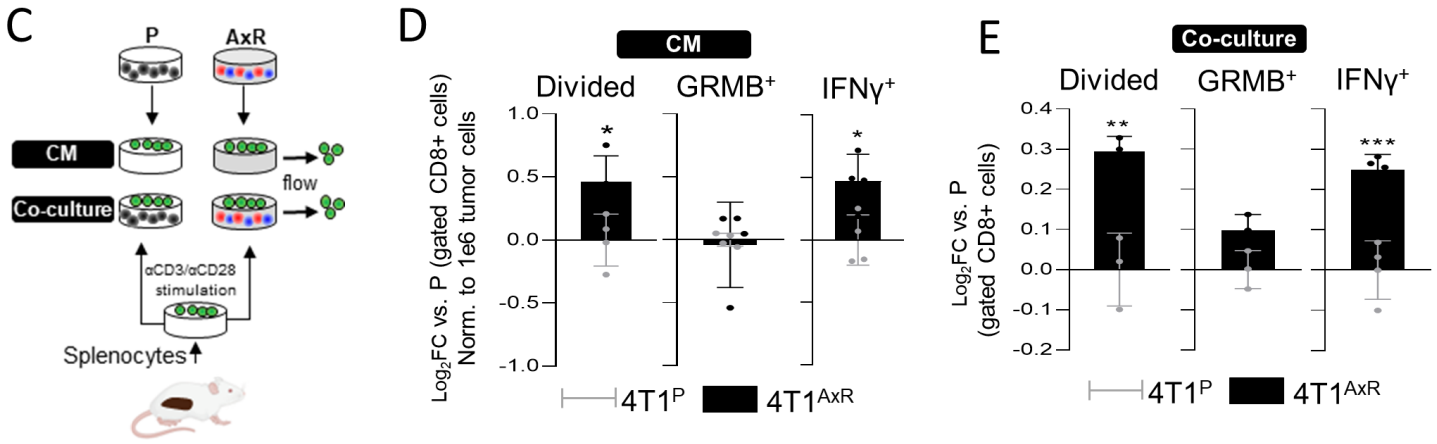
C
P
AxR
CM
Co-culture
flow
αCD3/αCD28 stimulation
Splenocytes
D
CM
Divided
GRMB+
IFNγ+
Log2FC vs. P (gated CD8+ cells) Norm. to 1e6 tumor cells
4T1P
4T1AxR
E
Co-culture
Divided
GRMB+
IFNγ+
Log2FC vs. P (gated CD8+ cells)
4T1P
4T1AxR

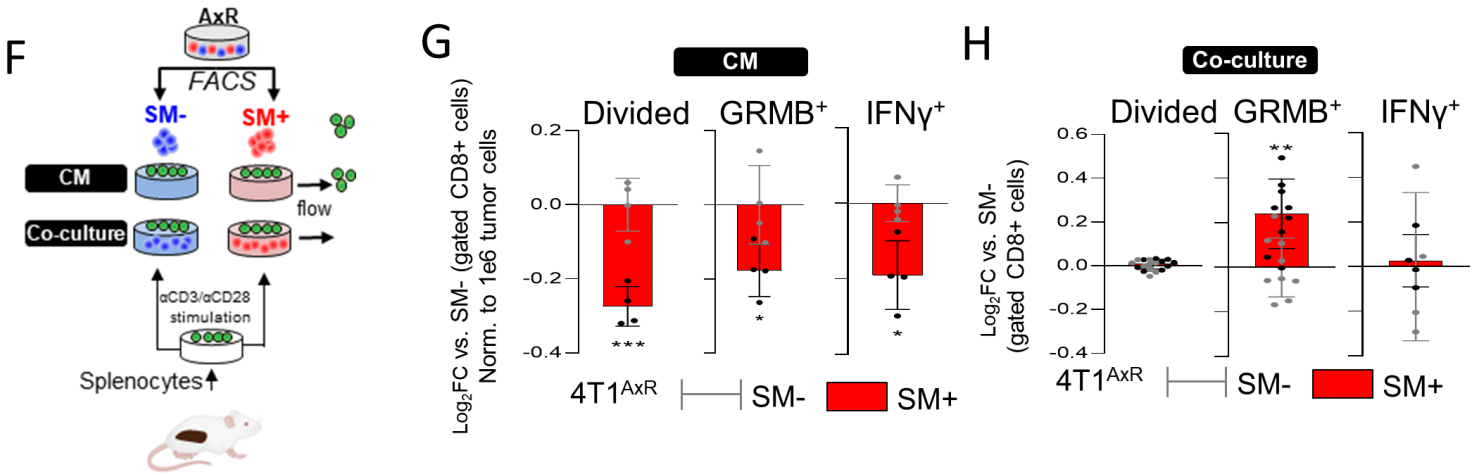
F
AxR
FACS
SM-
SM+
CM
Co-culture
flow
αCD3/αCD28 stimulation
Splenocytes
G
CM
Divided
GRMB+
IFNγ+
Log2FC vs. SM- (gated CD8+ cells) Norm. to 1e6 tumor cells
4T1AxR
SM-
SM+
H
Co-culture
Divided
GRMB+
IFNγ+
Log2FC vs. SM- (gated CD8+ cells)
4T1AxR
SM-
SM+

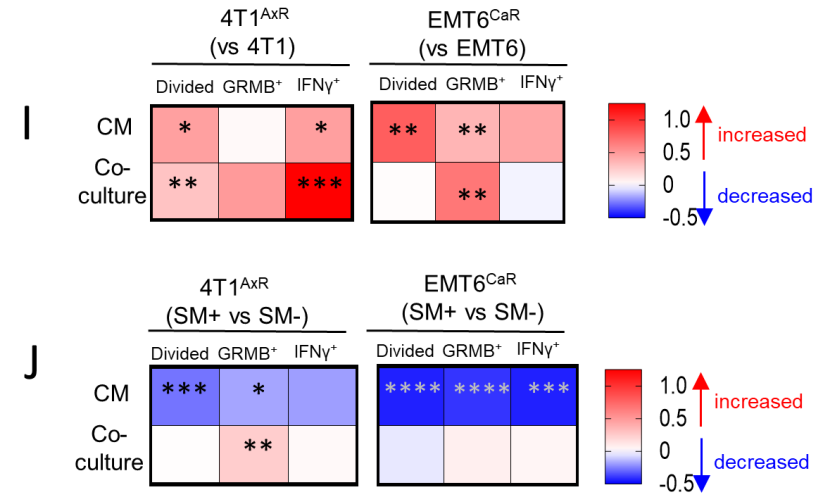
I
4T1AxR (vs 4T1)
EMT6CaR (vs EMT6)
Divided GRMB+ IFNγ+
CM
Co-culture
increased
decreased
J
4T1AxR (SM+ vs SM-)
EMT6CaR (SM+ vs SM-)
Divided GRMB+ IFNγ+
CM
Co-culture
increased
decreased

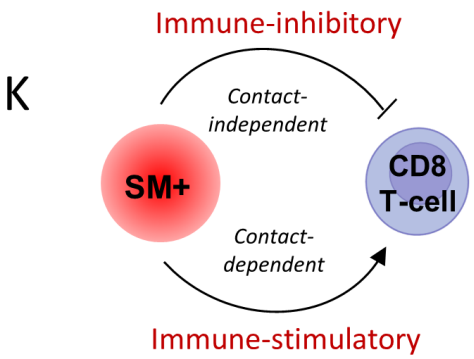
K
Immune-inhibitory
Contact-independent
SM+
CD8 T-cell
Contact-dependent
Immune-stimulatory

Figure 6

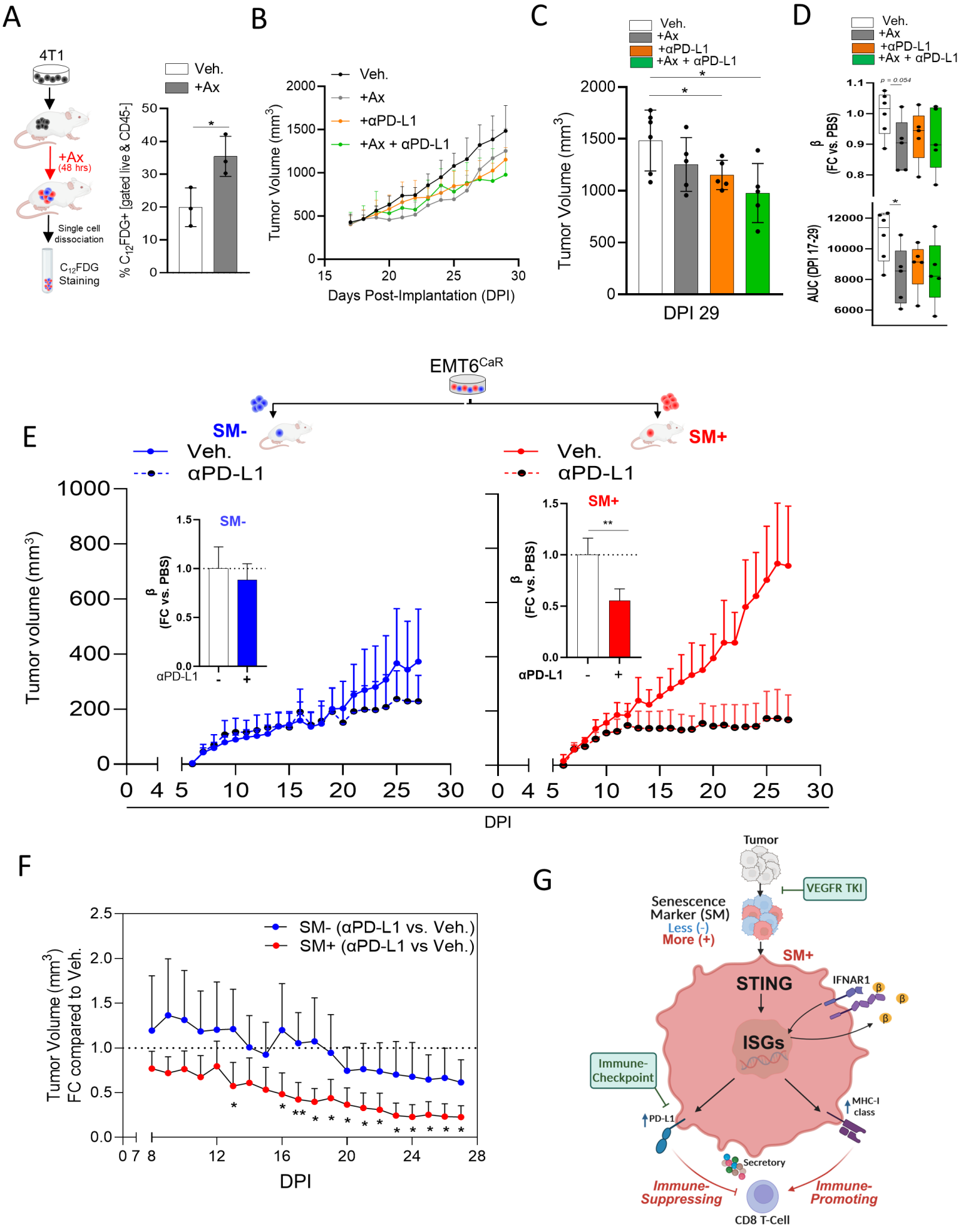
A
4T1
+Ax
(48 hrs)
Single cell
dissociation
C12FDG
Staining
Veh.
+Ax
% C12FDG+ [gated live & CD45-]
B
Veh.
+Ax
+αPD-L1
+Ax + αPD-L1
Tumor Volume (mm3)
Days Post-Implantation (DPI)
C
Veh.
+Ax
+αPD-L1
+Ax + αPD-L1
Tumor Volume (mm3)
DPI 29
D
Veh.
+Ax
+αPD-L1
+Ax + αPD-L1
β (FC vs. PBS)
AUC (DPI 17-29)
E
EMT6CaR
SM-
SM+
Veh.
αPD-L1
Tumor volume (mm3)
β (FC vs. PBS)
αPD-L1
DPI
F
SM- (αPD-L1 vs. Veh.)
SM+ (αPD-L1 vs Veh.)
Tumor Volume (mm3)
FC compared to Veh.
DPI
G
Tumor
VEGFR TKI
Senescence
Marker (SM)
Less (-)
More (+)
SM+
STING
IFNAR1
ISGs
Immune-
Checkpoint
PD-L1
MHC-I
class
Secretory
Immune-
Suppressing
Immune-
Promoting
CD8 T-Cell

Parsed Citations

1. Upadhaya, S., Neftelinov, S.T., Hodge, J., and Campbell, J. (2022). Challenges and opportunities in the PD1/PDL1 inhibitor clinical trial landscape. Nat Rev Drug Discov. 10.1038/d41573-022- 00030-4.
Pubmed: Author and Title
Google Scholar: Google Scholar Search

2. Vafaei, S., Zekiy, A.O., Khanamir, R.A., Zaman, B.A., Ghayourvahdat, A., Azimizonuzi, H., and Zamani, M. (2022). Combination therapy with immune checkpoint inhibitors (ICIs); a new frontier. Cancer Cell Int 22, 2. 10.1186/s12935-021-02407-8.
Pubmed: Author and Title
Google Scholar: Google Scholar Search

3. Varayathu, H., Sarathy, V., Thomas, B.E., Mufti, S.S., and Naik, R. (2021). Combination Strategies to Augment Immune Check Point Inhibitors Efficacy - Implications for Translational Research. Front Oncol 11, 559161. 10.3389/fonc.2021.559161.
Pubmed: Author and Title
Google Scholar: Google Scholar Search

4. Kohli, J., Wang, B., Brandenburg, S.M., Basisty, N., Evangelou, K., Varela-Eirin, M., Campisi, J., Schilling, B., Gorgoulis, V., and Demaria, M. (2021). Algorithmic assessment of cellular senescence in experimental and clinical specimens. Nat Protoc 16, 2471-2498. 10.1038/s41596- 021-00505-5.
Pubmed: Author and Title
Google Scholar: Google Scholar Search

5. Gonzalez-Gualda, E., Baker, A.G., Fruk, L., and Munoz-Espin, D. (2021). A guide to assessing cellular senescence in vitro and in vivo. FEBS J 288, 56-80. 10.1111/febs.15570.
Pubmed: Author and Title
Google Scholar: Google Scholar Search

6. Davan-Wetton, C.S.A., Pessolano, E., Perretti, M., and Montero-Melendez, T. (2021). Senescence under appraisal: hopes and challenges revisited. Cell Mol Life Sci 78, 3333-3354.
Pubmed: Author and Title
Google Scholar: Google Scholar Search

10.1007/s00018-020-03746-x.

7. Mastri, M., Tracz, A., Lee, C.R., Dolan, M., Attwood, K., Christensen, J.G., Liu, S., and Ebos, J.M.L. (2018). A Transient Pseudosenescent Secretome Promotes Tumor Growth after Antiangiogenic Therapy Withdrawal. Cell Rep 25, 3706-3720 e3708.
Pubmed: Author and Title
Google Scholar: Google Scholar Search

10.1016/j.celrep.2018.12.017.

8. Mastri, M., and Ebos, J.M.L. (2019). Tumor growth fueled by spurious senescence phenotypes. Mol Cell Oncol 6, 1575707. 10.1080/23723556.2019.1575707.
Pubmed: Author and Title
Google Scholar: Google Scholar Search

9. Sharpless, N.E., and Sherr, C.J. (2015). Forging a signature of in vivo senescence. Nat Rev Cancer 15, 397-408. 10.1038/nrc3960.
Pubmed: Author and Title
Google Scholar: Google Scholar Search

10. Ewald, J.A., Desotelle, J.A., Wilding, G., and Jarrard, D.F. (2010). Therapy-induced senescence in cancer. J Natl Cancer Inst 102, 1536-1546. 10.1093/jnci/djq364.
Pubmed: Author and Title
Google Scholar: Google Scholar Search

11. Coppe, J.P., Desprez, P.Y., Krtolica, A., and Campisi, J. (2010). The senescence-associated secretory phenotype: the dark side of tumor suppression. Annual review of pathology 5, 99-118.
Pubmed: Author and Title
Google Scholar: Google Scholar Search

10.1146/annurev-pathol-121808-102144.

12. Ruscetti, M., Morris, J.P.t., Mezzadra, R., Russell, J., Leibold, J., Romesser, P.B., Simon, J., Kulick, A., Ho, Y.J., Fennell, M., et al. (2020). Senescence-Induced Vascular Remodeling Creates Therapeutic Vulnerabilities in Pancreas Cancer. Cell 181, 424-441 e421.
Pubmed: Author and Title
Google Scholar: Google Scholar Search

10.1016/j.cell.2020.03.008.

13. Ruscetti, M., Leibold, J., Bott, M.J., Fennell, M., Kulick, A., Salgado, N.R., Chen, C.C., Ho, Y.J., Sanchez-Rivera, F.J., Feucht, J., et al. (2018). NK cell-mediated cytotoxicity contributes to tumor control by a cytostatic drug combination. Science 362, 1416-1422. 10.1126/science.aas9090.
Pubmed: Author and Title
Google Scholar: Google Scholar Search

14. Tonnessen-Murray, C.A., Frey, W.D., Rao, S.G., Shahbandi, A., Ungerleider, N.A., Olayiwola, J.O., Murray, L.B., Vinson, B.T., Chrisey, D.B., Lord, C.J., and Jackson, J.G. (2019). Chemotherapy-induced senescent cancer cells engulf other cells to enhance their survival. J Cell Biol 218, 3827-3844. 10.1083/jcb.201904051.
Pubmed: Author and Title
Google Scholar: Google Scholar Search

15. Duy, C., Li, M., Teater, M., Meydan, C., Garrett-Bakelman, F.E., Lee, T.C., Chin, C.R., Durmaz, C., Kawabata, K.C., Dhimolea, E., et al. (2021). Chemotherapy Induces Senescence-Like Resilient Cells Capable of Initiating AML Recurrence. Cancer Discov 11, 1542-1561.
Pubmed: Author and Title
Google Scholar: Google Scholar Search

10.1158/2159-8290.CD-20-1375.
Pubmed: Author and Title
Google Scholar: Google Scholar Search

16. Choi, Y.W., Kim, Y.H., Oh, S.Y., Suh, K.W., Kim, Y.S., Lee, G.Y., Yoon, J.E., Park, S.S., Lee, Y.K., Park, Y.J., et al. (2021). Senescent Tumor Cells Build a Cytokine Shield in Colorectal Cancer. Adv Sci (Weinh) 8, 2002497. 10.1002/advs.202002497.
Pubmed: Author and Title
Google Scholar: Google Scholar Search

17. Iannello, A., Thompson, T.W., Ardolino, M., Lowe, S.W., and Raulet, D.H. (2013). p53- dependent chemokine production by senescent tumor cells supports NKG2D-dependent tumor elimination by natural killer cells. J Exp Med 210, 2057-2069. 10.1084/jem.20130783.
Pubmed: Author and Title
Google Scholar: Google Scholar Search

18. Ovadya, Y., Landsberger, T., Leins, H., Vadai, E., Gal, H., Biran, A., Yosef, R., Sagiv, A., Agrawal, A., Shapira, A., et al. (2018). Impaired immune surveillance accelerates accumulation of senescent cells and aging. Nat Commun 9, 5435. 10.1038/s41467-018-07825-3.
Pubmed: Author and Title
Google Scholar: Google Scholar Search

19. Cerboni, C., Fionda, C., Soriani, A., Zingoni, A., Doria, M., Cippitelli, M., and Santoni, A. (2014). The DNA Damage Response: A Common Pathway in the Regulation of NKG2D and DNAM-1 Ligand Expression in Normal, Infected, and Cancer Cells. Front Immunol 4, 508.
Pubmed: Author and Title
Google Scholar: Google Scholar Search

10.3389/fimmu.2013.00508.
Pubmed: Author and Title
Google Scholar: Google Scholar Search

20. Krizhanovsky, V., Yon, M., Dickins, R.A., Hearn, S., Simon, J., Miething, C., Yee, H., Zender, L., and Lowe, S.W. (2008). Senescence of activated stellate cells limits liver fibrosis. Cell 134, 657-667. 10.1016/j.cell.2008.06.049.
Pubmed: Author and Title
Google Scholar: Google Scholar Search

21. Egashira, M., Hirota, Y., Shimizu-Hirota, R., Saito-Fujita, T., Haraguchi, H., Matsumoto, L., Matsuo, M., Hiraoka, T., Tanaka, T., Akaeda, S., et al. (2017). F4/80+ Macrophages Contribute to Clearance of Senescent Cells in the Mouse Postpartum Uterus. Endocrinology 158, 2344-2353.
Pubmed: Author and Title
Google Scholar: Google Scholar Search

10.1210/en.2016-1886.
Pubmed: Author and Title
Google Scholar: Google Scholar Search

22. Irvine, K.M., Skoien, R., Bokil, N.J., Melino, M., Thomas, G.P., Loo, D., Gabrielli, B., Hill, M.M., Sweet, M.J., Clouston, A.D., and Powell, E.E. (2014). Senescent human hepatocytes express a unique secretory phenotype and promote macrophage migration. World J Gastroenterol 20, 17851-17862. 10.3748/wjg.v20.i47.17851.
Pubmed: Author and Title
Google Scholar: Google Scholar Search

23. Xue, W., Zender, L., Miething, C., Dickins, R.A., Hernando, E., Krizhanovsky, V., Cordon- Cardo, C., and Lowe, S.W. (2007). Senescence and tumour clearance is triggered by p53 restoration in murine liver carcinomas. Nature 445, 656-660. 10.1038/nature05529.
Pubmed: Author and Title
Google Scholar: Google Scholar Search

24. Pereira, B.I., Devine, O.P., Vukmanovic-Stejic, M., Chambers, E.S., Subramanian, P., Patel, N., Virasami, A., Sebire, N.J., Kinsler, V., Valdovinos, A., et al. (2019). Senescent cells evade immune clearance via HLA-E-mediated NK and CD8(+) T cell inhibition. Nat Commun 10, 2387. 10.1038/s41467-019-10335-5.
Pubmed: Author and Title
Google Scholar: Google Scholar Search

25. Ruhland, M.K., Loza, A.J., Capietto, A.H., Luo, X., Knolhoff, B.L., Flanagan, K.C., Belt, B.A., Alspach, E., Leahy, K., Luo, J., et al. (2016). Stromal senescence establishes an immunosuppressive microenvironment that drives tumorigenesis. Nat Commun 7, 11762.
Pubmed: Author and Title
Google Scholar: Google Scholar Search

10.1038/ncomms11762.

26. Garcia-Diaz, A., Shin, D.S., Moreno, B.H., Saco, J., Escuin-Ordinas, H., Rodriguez, G.A., Zaretsky, J.M., Sun, L., Hugo, W., Wang, X., et al. (2017). Interferon Receptor Signaling Pathways Regulating PD-L1 and PD-L2 Expression. Cell reports 19, 1189-1201.
Pubmed: Author and Title
Google Scholar: Google Scholar Search

10.1016/j.celrep.2017.04.031.

27. Yu, Q., Katlinskaya, Y.V., Carbone, C.J., Zhao, B., Katlinski, K.V., Zheng, H., Guha, M., Li, N., Chen, Q., Yang, T., et al. (2015). DNA-damage-induced type I interferon promotes senescence and inhibits stem cell function. Cell Rep 11, 785-797. 10.1016/j.celrep.2015.03.069.
Pubmed: Author and Title
Google Scholar: Google Scholar Search

28. Frisch, S.M., and MacFawn, I.P. (2020). Type I interferons and related pathways in cell senescence. Aging Cell 19, e13234. 10.1111/acel.13234.
Pubmed: Author and Title
Google Scholar: Google Scholar Search

29. Takahashi, A., Loo, T.M., Okada, R., Kamachi, F., Watanabe, Y., Wakita, M., Watanabe, S., Kawamoto, S., Miyata, K., Barber, G.N., et al. (2018). Downregulation of cytoplasmic DNases is implicated in cytoplasmic DNA accumulation and SASP in senescent cells. Nat Commun 9, 1249. 10.1038/s41467-018-03555-8.
Pubmed: Author and Title
Google Scholar: Google Scholar Search

30. Dunphy, G., Flannery, S.M., Almine, J.F., Connolly, D.J., Paulus, C., Jonsson, K.L., Jakobsen, M.R., Nevels, M.M., Bowie, A.G., and Unterholzner, L. (2018). Non-canonical Activation of the DNA Sensing Adaptor STING by ATM and IFI16 Mediates NF-kappaB Signaling after Nuclear DNA Damage. Mol Cell 71, 745-760 e745. 10.1016/j.molcel.2018.07.034.
Pubmed: Author and Title
Google Scholar: Google Scholar Search

31. Yang, H., Wang, H., Ren, J., Chen, Q., and Chen, Z.J. (2017). cGAS is essential for cellular senescence. Proc Natl Acad Sci U S A 114, E4612-E4620. 10.1073/pnas.1705499114.
Pubmed: Author and Title
Google Scholar: Google Scholar Search

32. Falahat, R., Perez-Villarroel, P., Mailloux, A.W., Zhu, G., Pilon-Thomas, S., Barber, G.N., and Mule, J.J. (2019). STING Signaling in Melanoma Cells Shapes Antigenicity and Can Promote Antitumor T-cell Activity. Cancer immunology research 7, 1837-1848. 10.1158/2326-6066.CIR- 19-0229.
Pubmed: Author and Title
Google Scholar: Google Scholar Search

33. Brenner, E., Schorg, B.F., Ahmetlic, F., Wieder, T., Hilke, F.J., Simon, N., Schroeder, C., Demidov, G., Riedel, T., Fehrenbacher, B., et al. (2020). Cancer immune control needs senescence induction by interferon-dependent cell cycle regulator pathways in tumours. Nat Commun 11, 1335. 10.1038/s41467-020-14987-6.
Pubmed: Author and Title
Google Scholar: Google Scholar Search

34. Abe, T., and Barber, G.N. (2014). Cytosolic-DNA-mediated, STING-dependent proinflammatory gene induction necessitates canonical NF-kappaB activation through TBK1. J Virol 88, 5328- 5341. 10.1128/JVI.00037-14.
Pubmed: Author and Title
Google Scholar: Google Scholar Search

35. Woo, S.R., Fuertes, M.B., Corrales, L., Spranger, S., Furdyna, M.J., Leung, M.Y., Duggan, R., Wang, Y., Barber, G.N., Fitzgerald, K.A., et al. (2014). STING-dependent cytosolic DNA sensing mediates innate immune recognition of immunogenic tumors. Immunity 41, 830-842.
Pubmed: Author and Title
Google Scholar: Google Scholar Search

10.1016/j.immuni.2014.10.017.

36. Ishikawa, H., and Barber, G.N. (2008). STING is an endoplasmic reticulum adaptor that facilitates innate immune signalling. Nature 455, 674-678. 10.1038/nature07317.
Pubmed: Author and Title
Google Scholar: Google Scholar Search

37. Georgilis, A., and Gil, J. (2016). Controlling secretion to limit chemoresistance. Genes Dev 30, 1791-1792. 10.1101/gad.288571.116.
Pubmed: Author and Title
Google Scholar: Google Scholar Search

38. Velarde, M.C., and Demaria, M. (2016). Targeting Senescent Cells: Possible Implications for Delaying Skin Aging: A Mini-Review. Gerontology 62, 513-518. 10.1159/000444877.
Pubmed: Author and Title
Google Scholar: Google Scholar Search

39. Tchkonia, T., Zhu, Y., van Deursen, J., Campisi, J., and Kirkland, J.L. (2013). Cellular senescence and the senescent secretory phenotype: therapeutic opportunities. J Clin Invest 123, 966-972. 10.1172/JCI64098.
Pubmed: Author and Title
Google Scholar: Google Scholar Search

40. de Keizer, P.L. (2017). The Fountain of Youth by Targeting Senescent Cells? Trends Mol Med 23, 6-17. 10.1016/j.molmed.2016.11.006.
Pubmed: Author and Title
Google Scholar: Google Scholar Search

41. Juers, D.H., Matthews, B.W., and Huber, R.E. (2012). LacZ beta-galactosidase: structure and function of an enzyme of historical and molecular biological importance. Protein Sci 21, 1792- 1807. 10.1002/pro.2165.
Pubmed: Author and Title
Google Scholar: Google Scholar Search

42. Debacq-Chainiaux, F., Erusalimsky, J.D., Campisi, J., and Toussaint, O. (2009). Protocols to detect senescence-associated beta-galactosidase (SA-betagal) activity, a biomarker of senescent cells in culture and in vivo. Nat Protoc 4, 1798-1806. 10.1038/nprot.2009.191.
Pubmed: Author and Title
Google Scholar: Google Scholar Search

43. Morelli, M.B., Amantini, C., Santoni, M., Soriani, A., Nabissi, M., Cardinali, C., Santoni, A., and Santoni, G. (2015). Axitinib induces DNA damage response leading to senescence, mitotic catastrophe, and increased NK cell recognition in human renal carcinoma cells. Oncotarget 6, 36245-36259. 10.18632/oncotarget.5768.
Pubmed: Author and Title
Google Scholar: Google Scholar Search

44. Coppe, J.P., Patil, C.K., Rodier, F., Sun, Y., Munoz, D.P., Goldstein, J., Nelson, P.S., Desprez, P.Y., and Campisi, J. (2008). Senescence-associated secretory phenotypes reveal cell- nonautonomous functions of oncogenic RAS and the p53 tumor suppressor. PLoS Biol 6, 2853- 2868. 10.1371/journal.pbio.0060301.
Pubmed: Author and Title
Google Scholar: Google Scholar Search

45. Rodier, F., Coppe, J.P., Patil, C.K., Hoeijmakers, W.A., Munoz, D.P., Raza, S.R., Freund, A., Campeau, E., Davalos, A.R., and Campisi, J. (2009). Persistent DNA damage signalling triggers senescence-associated inflammatory cytokine secretion. Nat Cell Biol 11, 973-979.
Pubmed: Author and Title
Google Scholar: Google Scholar Search

10.1038/ncb1909.

46. Bent, E.H., Gilbert, L.A., and Hemann, M.T. (2016). A senescence secretory switch mediated by PI3K/AKT/mTOR activation controls chemoprotective endothelial secretory responses. Genes Dev 30, 1811-1821. 10.1101/gad.284851.116.
Pubmed: Author and Title
Google Scholar: Google Scholar Search

47. Kuilman, T., Michaloglou, C., Vredeveld, L.C., Douma, S., van Doorn, R., Desmet, C.J., Aarden, L.A., Mooi, W.J., and Peeper, D.S. (2008). Oncogene-induced senescence relayed by an interleukin-dependent inflammatory network. Cell 133, 1019-1031. 10.1016/j.cell.2008.03.039.
Pubmed: Author and Title
Google Scholar: Google Scholar Search

48. Obenauf, A.C., Zou, Y., Ji, A.L., Vanharanta, S., Shu, W., Shi, H., Kong, X., Bosenberg, M.C., Wiesner, T., Rosen, N., et al. (2015). Therapy-induced tumour secretomes promote resistance and tumour progression. Nature 520, 368-372. 10.1038/nature14336.
Pubmed: Author and Title
Google Scholar: Google Scholar Search

49. Pribluda, A., Elyada, E., Wiener, Z., Hamza, H., Goldstein, R.E., Biton, M., Burstain, I., Morgenstern, Y., Brachya, G., Billauer, H., et al. (2013). A senescence-inflammatory switch from cancer-inhibitory to cancer-promoting mechanism. Cancer cell 24, 242-256.
Pubmed: Author and Title
Google Scholar: Google Scholar Search

10.1016/j.ccr.2013.06.005.

50. Kuilman, T., and Peeper, D.S. (2009). Senescence-messaging secretome: SMS-ing cellular stress. Nat Rev Cancer 9, 81-94. 10.1038/nrc2560.
Pubmed: Author and Title
Google Scholar: Google Scholar Search

51. Acosta, J.C., O'Loghlen, A., Banito, A., Guijarro, M.V., Augert, A., Raguz, S., Fumagalli, M., Da Costa, M., Brown, C., Popov, N., et al. (2008). Chemokine signaling via the CXCR2 receptor reinforces senescence. Cell 133, 1006-1018. 10.1016/j.cell.2008.03.038.
Pubmed: Author and Title
Google Scholar: Google Scholar Search

52. Rusinova, I., Forster, S., Yu, S., Kannan, A., Masse, M., Cumming, H., Chapman, R., and Hertzog, P.J. (2013). Interferome v2.0: an updated database of annotated interferon-regulated genes. Nucleic Acids Res 41, D1040-1046. 10.1093/nar/gks1215.
Pubmed: Author and Title
Google Scholar: Google Scholar Search

53. Grullich, C. (2018). Cabozantinib: Multi-kinase Inhibitor of MET, AXL, RET, and VEGFR2. Recent Results Cancer Res 211, 67-75. 10.1007/978-3-319-91442-8_5.
Pubmed: Author and Title
Google Scholar: Google Scholar Search

54. Wood, C.G., Ferguson, J.E., 3rd, Parker, J.S., Moore, D.T., Whisenant, J.G., Maygarden, S.J., Wallen, E.M., Kim, W.Y., Milowsky, M.I., Beckermann, K.E., et al. (2020). Neoadjuvant pazopanib and molecular analysis of tissue response in renal cell carcinoma. JCI Insight 5.
Pubmed: Author and Title
Google Scholar: Google Scholar Search

10.1172/jci.insight.132852.
Pubmed: Author and Title
Google Scholar: Google Scholar Search

55. Braga, S., Cardoso, J., Andre, S., Brito, M., Sanchez, P., Orvalho, L., Salgado, L., Dias, S., Pereira-Leal, J.B., and Passos-Coelho, J.L. (2017). Does Hypoxic Response Mediate Primary Resistance to Sunitinib in Untreated Locally Advanced Breast Cancer? Curr Cancer Drug Targets 17, 62-73. 10.2174/1568009616666161025114914.
Pubmed: Author and Title
Google Scholar: Google Scholar Search

56. Diaz-Montero, C.M., Mao, F.J., Barnard, J., Parker, Y., Zamanian-Daryoush, M., Pink, J.J., Finke, J.H., Rini, B.I., and Lindner, D.J. (2016). MEK inhibition abrogates sunitinib resistance in a renal cell carcinoma patient-derived xenograft model. Br J Cancer 115, 920-928.
Pubmed: Author and Title
Google Scholar: Google Scholar Search

10.1038/bjc.2016.263.

57. Pan, B.S., Perera, S.A., Piesvaux, J.A., Presland, J.P., Schroeder, G.K., Cumming, J.N., Trotter, B.W., Altman, M.D., Buevich, A.V., Cash, B., et al. (2020). An orally available non-nucleotide STING agonist with antitumor activity. Science 369. 10.1126/science.aba6098.
Pubmed: Author and Title
Google Scholar: Google Scholar Search

58. Prantner, D., Perkins, D.J., Lai, W., Williams, M.S., Sharma, S., Fitzgerald, K.A., and Vogel, S.N. (2012). 5,6-Dimethylxanthenone-4-acetic acid (DMXAA) activates stimulator of interferon gene (STING)-dependent innate immune pathways and is regulated by mitochondrial membrane potential. J Biol Chem 287, 39776-39788. 10.1074/jbc.M112.382986.
Pubmed: Author and Title
Google Scholar: Google Scholar Search

59. Conlon, J., Burdette, D.L., Sharma, S., Bhat, N., Thompson, M., Jiang, Z., Rathinam, V.A., Monks, B., Jin, T., Xiao, T.S., et al. (2013). Mouse, but not human STING, binds and signals in response to the vascular disrupting agent 5,6-dimethylxanthenone-4-acetic acid. J Immunol 190, 5216-5225. 10.4049/jimmunol.1300097.
Pubmed: Author and Title
Google Scholar: Google Scholar Search

60. Braumuller, H., Wieder, T., Brenner, E., Assmann, S., Hahn, M., Alkhaled, M., Schilbach, K., Essmann, F., Kneilling, M., Griessinger, C., et al. (2013). T-helper-1-cell cytokines drive cancer into senescence. Nature 494, 361-365. 10.1038/nature11824.
Pubmed: Author and Title
Google Scholar: Google Scholar Search

61. De Cecco, M., Ito, T., Petrashen, A.P., Elias, A.E., Skvir, N.J., Criscione, S.W., Caligiana, A., Brocculi, G., Adney, E.M., Boeke, J.D., et al. (2019). L1 drives IFN in senescent cells and promotes age-associated inflammation. Nature 566, 73-78. 10.1038/s41586-018-0784-9.
Pubmed: Author and Title
Google Scholar: Google Scholar Search

62. Trinchieri, G. (2010). Type I interferon: friend or foe? J Exp Med 207, 2053-2063.
Pubmed: Author and Title
Google Scholar: Google Scholar Search

10.1084/jem.20101664.
Pubmed: Author and Title
Google Scholar: Google Scholar Search

63. Fenton, S.E., Saleiro, D., and Platanias, L.C. (2021). Type I and II Interferons in the Anti-Tumor Immune Response. Cancers (Basel) 13. 10.3390/cancers13051037.
Pubmed: Author and Title
Google Scholar: Google Scholar Search

64. Marin, I., Boix, O., Garcia-Garijo, A., Sirois, I., Caballe, A., Zarzuela, E., Ruano, I., Attolini, C.S., Prats, N., Lopez-Dominguez, J.A., et al. (2023). Cellular Senescence Is Immunogenic and Promotes Antitumor Immunity. Cancer discovery 13, 410-431. 10.1158/2159-8290.CD-22-0523.
Pubmed: Author and Title
Google Scholar: Google Scholar Search

65. Vaghi, C., Rodallec, A., Fanciullino, R., Ciccolini, J., Mochel, J.P., Mastri, M., Poignard, C., Ebos, J.M.L., and Benzekry, S. (2020). Population modeling of tumor growth curves and the reduced Gompertz model improve prediction of the age of experimental tumors. PLoS Comput Biol 16, e1007178. 10.1371/journal.pcbi.1007178.
Pubmed: Author and Title
Google Scholar: Google Scholar Search

66. Quah, B.J., and Parish, C.R. (2010). The use of carboxyfluorescein diacetate succinimidyl ester (CFSE) to monitor lymphocyte proliferation. J Vis Exp. 10.3791/2259.
Pubmed: Author and Title
Google Scholar: Google Scholar Search

67. Medema, J.P., de Jong, J., Peltenburg, L.T., Verdegaal, E.M., Gorter, A., Bres, S.A., Franken, K.L., Hahne, M., Albar, J.P., Melief, C.J., and Offringa, R. (2001). Blockade of the granzyme B/perforin pathway through overexpression of the serine protease inhibitor PI-9/SPI-6 constitutes a mechanism for immune escape by tumors. Proc Natl Acad Sci U S A 98, 11515-11520.
Pubmed: Author and Title
Google Scholar: Google Scholar Search

10.1073/pnas.201398198.
Pubmed: Author and Title
Google Scholar: Google Scholar Search

68. Mosely, S.I., Prime, J.E., Sainson, R.C., Koopmann, J.O., Wang, D.Y., Greenawalt, D.M., Ahdesmaki, M.J., Leyland, R., Mullins, S., Pacelli, L., et al. (2017). Rational Selection of Syngeneic Preclinical Tumor Models for Immunotherapeutic Drug Discovery. Cancer immunology research 5, 29-41. 10.1158/2326-6066.CIR-16-0114.
Pubmed: Author and Title
Google Scholar: Google Scholar Search

69. Mall, C., Sckisel, G.D., Proia, D.A., Mirsoian, A., Grossenbacher, S.K., Pai, C.S., Chen, M., Monjazeb, A.M., Kelly, K., Blazar, B.R., and Murphy, W.J. (2016). Repeated PD-1/PD-L1 monoclonal antibody administration induces fatal xenogeneic hypersensitivity reactions in a murine model of breast cancer. Oncoimmunology 5, e1075114.
Pubmed: Author and Title
Google Scholar: Google Scholar Search

10.1080/2162402X.2015.1075114.
Pubmed: Author and Title
Google Scholar: Google Scholar Search

70. Monjazeb, A.M., Wang, Z., Vick, L.V., Dunai, C., Minnar, C., Khuat, L.T., and Murphy, W.J. (2021). Mouse Preclinical Cancer Immunotherapy Modeling Involving Anti-PD-1 Therapies Reveals the Need to Use Mouse Reagents to Mirror Clinical Paradigms. Cancers (Basel) 13.
Pubmed: Author and Title
Google Scholar: Google Scholar Search

10.3390/cancers13040729.

71. Motzer, R.J., Penkov, K., Haanen, J., Rini, B., Albiges, L., Campbell, M.T., Venugopal, B., Kollmannsberger, C., Negrier, S., Uemura, M., et al. (2019). Avelumab plus Axitinib versus Sunitinib for Advanced Renal-Cell Carcinoma. N Engl J Med 380, 1103-1115.
Pubmed: Author and Title
Google Scholar: Google Scholar Search

10.1056/NEJMoa1816047.

72. Rini, B.I., Plimack, E.R., Stus, V., Gafanov, R., Hawkins, R., Nosov, D., Pouliot, F., Alekseev, B., Soulieres, D., Melichar, B., et al. (2019). Pembrolizumab plus Axitinib versus Sunitinib for Advanced Renal-Cell Carcinoma. N Engl J Med 380, 1116-1127. 10.1056/NEJMoa1816714.
Pubmed: Author and Title
Google Scholar: Google Scholar Search

73. Motzer, R.J., Robbins, P.B., Powles, T., Albiges, L., Haanen, J.B., Larkin, J., Mu, X.J., Ching, K.A., Uemura, M., Pal, S.K., et al. (2020). Avelumab plus axitinib versus sunitinib in advanced renal cell carcinoma: biomarker analysis of the phase 3 JAVELIN Renal 101 trial. Nat Med.
Pubmed: Author and Title
Google Scholar: Google Scholar Search

10.1038/s41591-020-1044-8.

74. Choueiri, T.K., Powles, T., Burotto, M., Escudier, B., Bourlon, M.T., Zurawski, B., Oyervides Juarez, V.M., Hsieh, J.J., Basso, U., Shah, A.Y., et al. (2021). Nivolumab plus Cabozantinib versus Sunitinib for Advanced Renal-Cell Carcinoma. N Engl J Med 384, 829-841.

Pubmed: Author and Title
Google Scholar: Google Scholar Search

10.1056/NEJMoa2026982.

75. Heine, A., Held, S.A., Bringmann, A., Holderried, T.A., and Brossart, P. (2011). Immunomodulatory effects of anti-angiogenic drugs. Leukemia 25, 899-905.
Pubmed: Author and Title
Google Scholar: Google Scholar Search

10.1038/leu.2011.24.

76. Stehle, F., Schulz, K., Fahldieck, C., Kalich, J., Lichtenfels, R., Riemann, D., and Seliger, B. (2013). Reduced immunosuppressive properties of axitinib in comparison with other tyrosine kinase inhibitors. J Biol Chem 288, 16334-16347. 10.1074/jbc.M112.437962.
Pubmed: Author and Title
Google Scholar: Google Scholar Search

77. Prasanna, P.G., Citrin, D.E., Hildesheim, J., Ahmed, M.M., Venkatachalam, S., Riscuta, G., Xi, D., Zheng, G., Deursen, J.V., Goronzy, J., et al. (2021). Therapy-Induced Senescence: Opportunities to Improve Anticancer Therapy. J Natl Cancer Inst 113, 1285-1298.
Pubmed: Author and Title
Google Scholar: Google Scholar Search

10.1093/jnci/djab064.

78. Wang, L., Lankhorst, L., and Bernards, R. (2022). Exploiting senescence for the treatment of cancer. Nat Rev Cancer 22, 340-355. 10.1038/s41568-022-00450-9.
Pubmed: Author and Title
Google Scholar: Google Scholar Search

79. Zhang, L., Pitcher, L.E., Prahalad, V., Niedernhofer, L.J., and Robbins, P.D. (2023). Targeting cellular senescence with senotherapeutics: senolytics and senomorphics. FEBS J 290, 1362-1383.
Pubmed: Author and Title
Google Scholar: Google Scholar Search

10.1111/febs.16350.
Pubmed: Author and Title
Google Scholar: Google Scholar Search

80. Wang, B., and Demaria, M. (2021). The Quest to Define and Target Cellular Senescence in Cancer. Cancer Res 81, 6087-6089. 10.1158/0008-5472.CAN-21-2032.
Pubmed: Author and Title
Google Scholar: Google Scholar Search

81. Lee, S., and Schmitt, C.A. (2019). The dynamic nature of senescence in cancer. Nat Cell Biol 21, 94-101. 10.1038/s41556-018-0249-2.
Pubmed: Author and Title
Google Scholar: Google Scholar Search

82. Chakradeo, S., Elmore, L.W., and Gewirtz, D.A. (2016). Is Senescence Reversible? Curr Drug Targets 17, 460-466.
Pubmed: Author and Title
Google Scholar: Google Scholar Search

83. Romaniello, D., Gelfo, V., Pagano, F., Ferlizza, E., Sgarzi, M., Mazzeschi, M., Morselli, A., Miano, C., D'Uva, G., and Lauriola, M. (2022). Senescence-associated reprogramming induced by interleukin-1 impairs response to EGFR neutralization. Cell Mol Biol Lett 27, 20.
Pubmed: Author and Title
Google Scholar: Google Scholar Search

10.1186/s11658-022-00319-7.

84. Salunkhe, S., Mishra, S.V., Nair, J., Shah, S., Gardi, N., Thorat, R., Sarkar, D., Rajendra, J., Kaur, E., and Dutt, S. (2021). Nuclear localization of p65 reverses therapy-induced senescence. J Cell Sci 134. 10.1242/jcs.253203.
Pubmed: Author and Title
Google Scholar: Google Scholar Search

85. Bollard, J., Miguela, V., Ruiz de Galarreta, M., Venkatesh, A., Bian, C.B., Roberto, M.P., Tovar, V., Sia, D., Molina-Sanchez, P., Nguyen, C.B., et al. (2017). Palbociclib (PD-0332991), a selective CDK4/6 inhibitor, restricts tumour growth in preclinical models of hepatocellular carcinoma. Gut 66, 1286-1296. 10.1136/gutjnl-2016-312268.
Pubmed: Author and Title
Google Scholar: Google Scholar Search

86. Maskey, R.S., Wang, F., Lehman, E., Wang, Y., Emmanuel, N., Zhong, W., Jin, G., Abraham, R.T., Arndt, K.T., Myers, J.S., and Mazurek, A. (2021). Sustained mTORC1 activity during palbociclib-induced growth arrest triggers senescence in ER+ breast cancer cells. Cell Cycle 20, 65-80. 10.1080/15384101.2020.1859195.
Pubmed: Author and Title
Google Scholar: Google Scholar Search

87. Fleury, H., Malaquin, N., Tu, V., Gilbert, S., Martinez, A., Olivier, M.A., Sauriol, A., Communal, L., Leclerc-Desaulniers, K., Carmona, E., et al. (2019). Exploiting interconnected synthetic lethal interactions between PARP inhibition and cancer cell reversible senescence. Nat Commun 10, 2556. 10.1038/s41467-019-10460-1.
Pubmed: Author and Title
Google Scholar: Google Scholar Search

88. Madorsky Rowdo, F.P., Baron, A., von Euw, E.M., and Mordoh, J. (2017). In vitro long-term treatment with MAPK inhibitors induces melanoma cells with resistance plasticity to inhibitors while retaining sensitivity to CD8 T cells. Oncol Rep 37, 1367-1378. 10.3892/or.2017.5363.
Pubmed: Author and Title
Google Scholar: Google Scholar Search

89. Kurppa, K.J., Liu, Y., To, C., Zhang, T., Fan, M., Vajdi, A., Knelson, E.H., Xie, Y., Lim, K., Cejas, P., et al. (2020). Treatment-Induced Tumor Dormancy through YAP-Mediated Transcriptional Reprogramming of the Apoptotic Pathway. Cancer Cell 37, 104-122 e112.
Pubmed: Author and Title
Google Scholar: Google Scholar Search

10.1016/j.ccell.2019.12.006.

90. Hu, Z., Yuan, J., Long, M., Jiang, J., Zhang, Y., Zhang, T., Xu, M., Fan, Y., Tanyi, J.L., Montone, K.T., et al. (2021). The Cancer Surfaceome Atlas integrates genomic, functional and drug response data to identify actionable targets. Nat Cancer 2, 1406-1422. 10.1038/s43018-021- 00282-w.
Pubmed: Author and Title
Google Scholar: Google Scholar Search

91. Saleh, T., Tyutyunyk-Massey, L., Murray, G.F., Alotaibi, M.R., Kawale, A.S., Elsayed, Z., Henderson, S.C., Yakovlev, V., Elmore, L.W., Toor, A., et al. (2019). Tumor cell escape from therapy-induced senescence. Biochem Pharmacol 162, 202-212. 10.1016/j.bcp.2018.12.013.
Pubmed: Author and Title
Google Scholar: Google Scholar Search

92. Hao, X., Zhao, B., Zhou, W., Liu, H., Fukumoto, T., Gabrilovich, D., and Zhang, R. (2021). Sensitization of ovarian tumor to immune checkpoint blockade by boosting senescence-associated secretory phenotype. iScience 24, 102016. 10.1016/j.isci.2020.102016.
Pubmed: Author and Title
Google Scholar: Google Scholar Search

93. Paffenholz, S.V., Salvagno, C., Ho, Y.J., Limjoco, M., Baslan, T., Tian, S., Kulick, A., de Stanchina, E., Wilkinson, J.E., Barriga, F.M., et al. (2022). Senescence induction dictates response to chemo- and

immunotherapy in preclinical models of ovarian cancer. Proc Natl Acad Sci U S A 119. 10.1073/pnas.2117754119.
Pubmed: Author and Title
Google Scholar: Google Scholar Search

94. Pantelidou, C., Sonzogni, O., De Oliveria Taveira, M., Mehta, A.K., Kothari, A., Wang, D., Visal, T., Li, M.K., Pinto, J., Castrillon, J.A., et al. (2019). PARP Inhibitor Efficacy Depends on CD8(+) T-cell Recruitment via Intratumoral STING Pathway Activation in BRCA-Deficient Models of Triple-Negative Breast Cancer. Cancer Discov 9, 722-737. 10.1158/2159-8290.CD-18- 1218.
Pubmed: Author and Title
Google Scholar: Google Scholar Search

95. Jing, W., McAllister, D., Vonderhaar, E.P., Palen, K., Riese, M.J., Gershan, J., Johnson, B.D., and Dwinell, M.B. (2019). STING agonist inflames the pancreatic cancer immune microenvironment and reduces tumor burden in mouse models. J Immunother Cancer 7, 115.
Pubmed: Author and Title
Google Scholar: Google Scholar Search

10.1186/s40425-019-0573-5.

96. Sistigu, A., Yamazaki, T., Vacchelli, E., Chaba, K., Enot, D.P., Adam, J., Vitale, I., Goubar, A., Baracco, E.E., Remedios, C., et al. (2014). Cancer cell-autonomous contribution of type I interferon signaling to the efficacy of chemotherapy. Nat Med 20, 1301-1309. 10.1038/nm.3708.
Pubmed: Author and Title
Google Scholar: Google Scholar Search

97. Adachi, Y., Kamiyama, H., Ichikawa, K., Fukushima, S., Ozawa, Y., Yamaguchi, S., Goda, S., Kimura, T., Kodama, K., Matsuki, M., et al. (2022). Inhibition of FGFR Reactivates IFNgamma Signaling in Tumor Cells to Enhance the Combined Antitumor Activity of Lenvatinib with Anti- PD-1 Antibodies. Cancer Res 82, 292-306. 10.1158/0008-5472.CAN-20-2426.
Pubmed: Author and Title
Google Scholar: Google Scholar Search

98. Goel, S., DeCristo, M.J., Watt, A.C., BrinJones, H., Sceneay, J., Li, B.B., Khan, N., Ubellacker, J.M., Xie, S., Metzger-Filho, O., et al. (2017). CDK4/6 inhibition triggers anti-tumour immunity. Nature 548, 471-475. 10.1038/nature23465.
Pubmed: Author and Title
Google Scholar: Google Scholar Search

99. Yang, H., Lee, W.S., Kong, S.J., Kim, C.G., Kim, J.H., Chang, S.K., Kim, S., Kim, G., Chon, H.J., and Kim, C. (2019). STING activation reprograms tumor vasculatures and synergizes with VEGFR2 blockade. J Clin Invest 129, 4350-4364. 10.1172/JCI125413.
Pubmed: Author and Title
Google Scholar: Google Scholar Search

100. Dimri, G.P., Lee, X., Basile, G., Acosta, M., Scott, G., Roskelley, C., Medrano, E.E., Linskens, M., Rubelj, I., Pereira-Smith, O., and et al. (1995). A biomarker that identifies senescent human cells in culture and in aging skin in vivo. Proc Natl Acad Sci U S A 92, 9363-9367.
Pubmed: Author and Title
Google Scholar: Google Scholar Search

10.1073/pnas.92.20.9363.
Pubmed: Author and Title
Google Scholar: Google Scholar Search

101. Kurz, D.J., Decary, S., Hong, Y., and Erusalimsky, J.D. (2000). Senescence-associated (beta)-galactosidase reflects an increase in lysosomal mass during replicative ageing of human endothelial cells. J Cell Sci 113 (Pt 20), 3613-3622. 10.1242/jcs.113.20.3613.
Pubmed: Author and Title
Google Scholar: Google Scholar Search

102. Lee, B.Y., Han, J.A., Im, J.S., Morrone, A., Johung, K., Goodwin, E.C., Kleijer, W.J., DiMaio, D., and Hwang, E.S. (2006). Senescence-associated beta-galactosidase is lysosomal beta- galactosidase. Aging Cell 5, 187-195. 10.1111/j.1474-9726.2006.00199.x.
Pubmed: Author and Title
Google Scholar: Google Scholar Search

103. Ruzickova, E., Skoupa, N., Dolezel, P., Smith, D.A., and Mlejnek, P. (2019). The Lysosomal Sequestration of Tyrosine Kinase Inhibitors and Drug Resistance. Biomolecules 9.
Pubmed: Author and Title
Google Scholar: Google Scholar Search

10.3390/biom9110675.

104. Gotink, K.J., Broxterman, H.J., Labots, M., de Haas, R.R., Dekker, H., Honeywell, R.J., Rudek, M.A., Beerepoot, L.V., Musters, R.J., Jansen, G., et al. (2011). Lysosomal sequestration of sunitinib: a novel mechanism of drug resistance. Clin Cancer Res 17, 7337-7346. 10.1158/1078- 0432.CCR-11-1667.
Pubmed: Author and Title
Google Scholar: Google Scholar Search

105. Fassl, A., Brain, C., Abu-Remaileh, M., Stukan, I., Butter, D., Stepien, P., Feit, A.S., Bergholz, J., Michowski, W., Otto, T., et al. (2020). Increased lysosomal biomass is responsible for the resistance of triple-negative breast cancers to CDK4/6 inhibition. Sci Adv 6, eabb2210.
Pubmed: Author and Title
Google Scholar: Google Scholar Search

10.1126/sciadv.abb2210.
Pubmed: Author and Title
Google Scholar: Google Scholar Search

106. Colombo, F., Trombetta, E., Cetrangolo, P., Maggioni, M., Razini, P., De Santis, F., Torrente, Y., Prati, D., Torresani, E., and Porretti, L. (2014). Giant Lysosomes as a Chemotherapy Resistance Mechanism in Hepatocellular Carcinoma Cells. PLoS One 9, e114787.
Pubmed: Author and Title
Google Scholar: Google Scholar Search

10.1371/journal.pone.0114787.
Pubmed: Author and Title
Google Scholar: Google Scholar Search

107. Zhang, H., Zoued, A., Liu, X., Sit, B., and Waldor, M.K. (2020). Type I interferon remodels lysosome function and modifies intestinal epithelial defense. Proc Natl Acad Sci U S A 117, 29862-29871. 10.1073/pnas.2010723117.
Pubmed: Author and Title
Google Scholar: Google Scholar Search

108. Unterholzner, L., and Dunphy, G. (2019). cGAS-independent STING activation in response to DNA damage. Mol Cell Oncol 6, 1558682. 10.1080/23723556.2018.1558682.
Pubmed: Author and Title
Google Scholar: Google Scholar Search

109. Elgendy, M., Abdel-Aziz, A.K., Renne, S.L., Bornaghi, V., Procopio, G., Colecchia, M., Kanesvaran, R., Toh, C.K., Bossi, D., Pallavicini, I., et al. (2017). Dual modulation of MCL-1 and mTOR determines the response to sunitinib. J Clin Invest 127, 153-168. 10.1172/JCI84386.
Pubmed: Author and Title
Google Scholar: Google Scholar Search

110. Jimenez-Valerio, G., Martinez-Lozano, M., Bassani, N., Vidal, A., Ochoa-de-Olza, M., Suarez, C., Garcia-Del-Muro, X., Carles, J., Vinals, F., Graupera, M., et al. (2016). Resistance to Antiangiogenic Therapies by Metabolic Symbiosis in Renal Cell Carcinoma PDX Models and Patients. Cell Rep 15, 1134-1143. 10.1016/j.celrep.2016.04.015.
Pubmed: Author and Title
Google Scholar: Google Scholar Search

111. Zhang, L., Wei, X., Wang, Z., Liu, P., Hou, Y., Xu, Y., Su, H., Koci, M.D., Yin, H., and Zhang, C. (2023). NF-kappaB activation enhances STING signaling by altering microtubule-mediated STING trafficking. Cell Rep 42, 112185. 10.1016/j.celrep.2023.112185.
Pubmed: Author and Title
Google Scholar: Google Scholar Search

112. Benci, J.L., Xu, B., Qiu, Y., Wu, T.J., Dada, H., Twyman-Saint Victor, C., Cucolo, L., Lee, D.S.M., Pauken, K.E., Huang, A.C., et al. (2016). Tumor Interferon Signaling Regulates a Multigenic Resistance Program to Immune Checkpoint Blockade. Cell 167, 1540-1554 e1512.
Pubmed: Author and Title
Google Scholar: Google Scholar Search

10.1016/j.cell.2016.11.022.

113. Shi, Y., Dolan, M., Mastri, M., Hill, J.W., Dommer, A., Benzekry, S., Eng, K., and Ebos, J.M.L. (2021). Acquired resistance to PD-L1 inhibition is associated with an enhanced type I IFN- stimulated secretory program in tumor cells. bioRxiv, 2021.2007.2001.450417.
Pubmed: Author and Title
Google Scholar: Google Scholar Search

10.1101/2021.07.01.450417.
Pubmed: Author and Title
Google Scholar: Google Scholar Search

114. Jacquelot, N., Yamazaki, T., Roberti, M.P., Duong, C.P.M., Andrews, M.C., Verlingue, L., Ferrere, G., Becharef, S., Vetizou, M., Daillere, R., et al. (2019). Sustained Type I interferon signaling as a mechanism of resistance to PD-1 blockade. Cell Res 29, 846-861. 10.1038/s41422- 019-0224-x.
Pubmed: Author and Title
Google Scholar: Google Scholar Search

115. Dolan, M., Mastri, M., Tracz, A., Christensen, J.G., Chatta, G., and Ebos, J.M.L. (2019). Enhanced efficacy of sitravatinib in metastatic models of antiangiogenic therapy resistance. PLoS One 14, e0220101. 10.1371/journal.pone.0220101.
Pubmed: Author and Title
Google Scholar: Google Scholar Search

116. Ebos, J.M., Mastri, M., Lee, C.R., Tracz, A., Hudson, J.M., Attwood, K., Cruz-Munoz, W.R., Jedeszko, C., Burns, P., and Kerbel, R.S. (2014). Neoadjuvant antiangiogenic therapy reveals contrasts in primary and metastatic tumor efficacy. EMBO Mol Med 6, 1561-1576.
Pubmed: Author and Title
Google Scholar: Google Scholar Search

10.15252/emmm.201403989.
Pubmed: Author and Title
Google Scholar: Google Scholar Search

117. Ebos, J.M., Lee, C.R., Bogdanovic, E., Alami, J., Van Slyke, P., Francia, G., Xu, P., Mutsaers, A.J., Dumont, D.J., and Kerbel, R.S. (2008). Vascular endothelial growth factor-mediated decrease in plasma soluble vascular endothelial growth factor receptor-2 levels as a surrogate biomarker for tumor growth. Cancer Res 68, 521-529. 10.1158/0008-5472.CAN-07-3217.
Pubmed: Author and Title
Google Scholar: Google Scholar Search

118. Tracz, A., Mastri, M., Lee, C.R., Pili, R., and Ebos, J.M. (2014). Modeling spontaneous metastatic renal cell carcinoma (mRCC) in mice following nephrectomy. J Vis Exp.
Pubmed: Author and Title
Google Scholar: Google Scholar Search

10.3791/51485.

119. Mundra, P.A., and Rajapakse, J.C. (2016). Gene and sample selection using T-score with sample selection. J Biomed Inform 59, 31-41. 10.1016/j.jbi.2015.11.003.

Pubmed: Author and Title
Google Scholar: Google Scholar Search